Volume 62
Number 34
5 May 2026
Pages 8521–8778

ChemComm

Chemical Communications

rsc.li/chemcomm

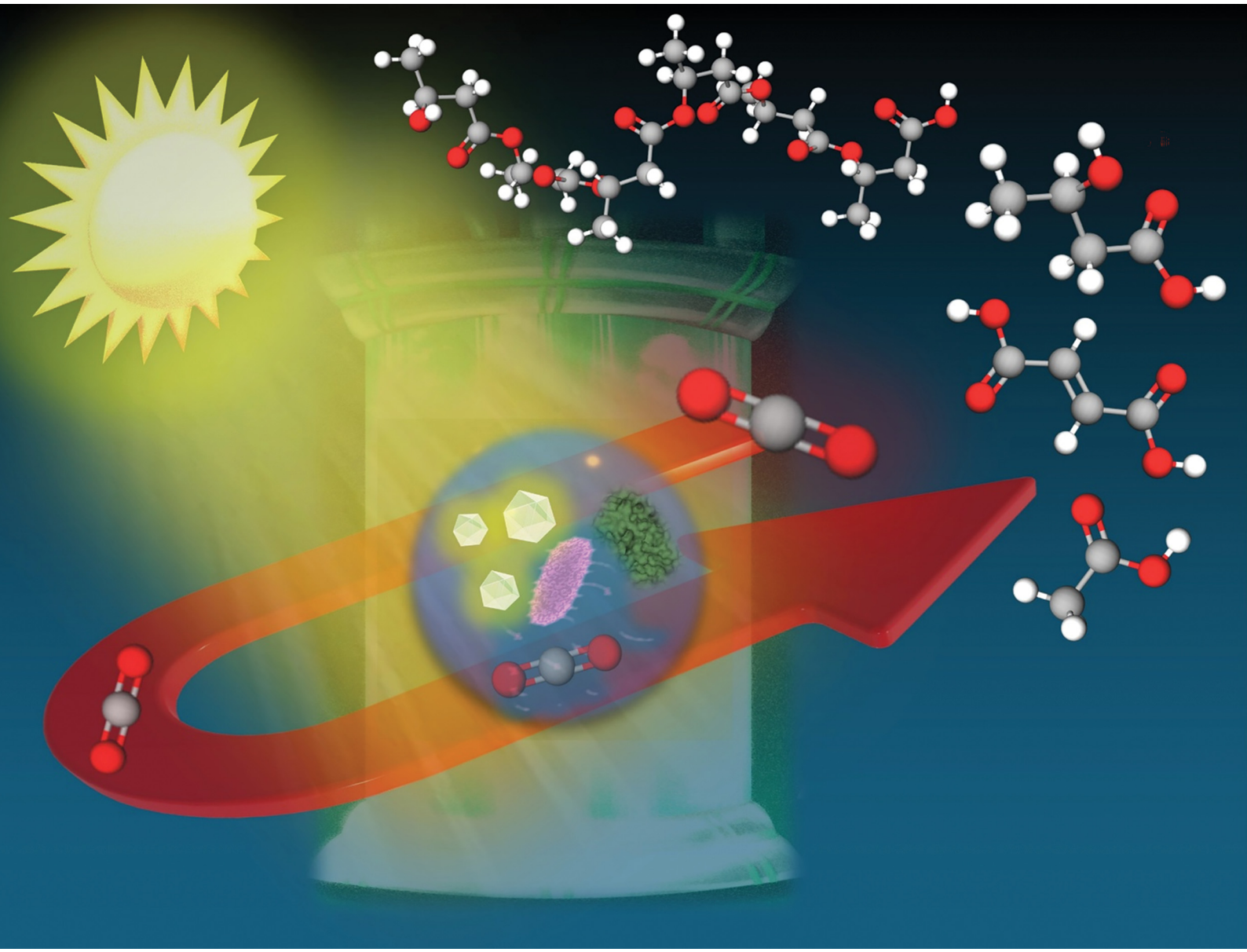

ISSN 1359-7345

ROYAL SOCIETY OF CHEMISTRY

REVIEW ARTICLE

Yutaka Amao *et al.*

CO_2-based biodegradable plastics and their precursor production using photo-biocatalytic processes

ChemComm

REVIEW ARTICLE

View Article Online
View Journal | View Issue

Cite this: *Chem. Commun.*, 2026, **62**, 8587

CO_2-based biodegradable plastics and their precursor production using photo-biocatalytic processes

Yu Kita,[a] Mika Takeuchi[b] and Yutaka Amao *[abc]

Biodegradable plastics are materials that can be decomposed by the action of microbes into water, CO_2, and biomass. They are attractive materials to solve the issue of serious environmental pollution due to plastic disposal. Some biodegradable plastics are produced entirely from petroleum-based precursors. The production of new biodegradable plastics and their precursors from CO_2 and persistent organic or bio-based compounds using visible-light driven redox with biocatalytic processes is one of the effective resolutions for the environmental issues of plastic pollution and global warming. In this review article, recent research on the visible-light driven production of CO_2-based biodegradable plastics and their precursors using a system of light-driven redox and biocatalytic processes is introduced. As a first example, an overview of research into the production of biodegradable plastics, poly(hydroxybutyrate) (PHB) and their precursors such as acetate, shikimic acid, acetoin and so on from CO_2 using a semiconductor photocatalyst-based photoredox system with a microbial cell as a biocatalytic process is provided. As a second example, an overview is provided of studies on the production of biodegradable plastic precursors, 3-hydroxybutyrate, L-malate and fumarate from CO_2 and small organic molecules using an organic dye-based photoredox system with an electron donor, an electron mediator and enzyme-based biocatalytic processes.

Received 16th January 2026,
Accepted 9th April 2026

DOI: 10.1039/d6cc00317f

rsc.li/chemcomm

[a] *Graduate School of Science, Osaka City University, Sugimoto 3-3-138, Sumiyoshi-ku, Osaka 558-8585, Japan*
[b] *Graduate School of Science, Osaka Metropolitan University, Sugimoto 3-3-138, Sumiyoshi-ku, Osaka 558-8585, Japan*
[c] *Research Centre for Artificial Photosynthesis, Osaka Metropolitan University, Sugimoto 3-3-138, Sumiyoshi-ku, Osaka 558-8585, Japan.*
E-mail: amao@omu.ac.jp

Introduction

Plastic is a versatile, lightweight, and relatively inexpensive material that has been an indispensable part of modern life.[1] Most plastics are made from fossil resources, primarily petroleum, and their entire manufacturing process lead to increasing

Yu Kita

Miss Yu Kita received her BSc and MSc from Osaka City University in 2020 and 2022, respectively, under the supervision of Professor Yutaka Amao. She has been working at Nippon Shokubai Co., Ltd since April 2023. Her research interest lies in the development of a solar-driven carbon dioxide-based synthesis system for biodegradable plastic precursors, such as 3-hydroxybutyrate, using a photo-/bio-hybrid catalyst system.

Mika Takeuchi

Miss Mika Takeuchi received her BSc from Osaka City University in 2021 and her MSc from Osaka Metropolitan University in 2023 under the supervision of Professor Yutaka Amao. She has been working at Daicel Corporation since April 2024. Her research interest in graduate school was the development of a solar-driven system for biodegradable plastic precursor production such as fumarate from carbon dioxide and biobased material using a photo/bio-hybrid catalyst.

greenhouse gas emissions.[2] Plastics pose environmental pollution concerns throughout their life cycle, from production to use and ultimately disposal.[3,4] However, plastics have a wide range of functions and are useful materials that support modern society, so it is necessary to establish methods for their production, use, and disposal without causing environmental pollution.[5] Accordingly, biodegradable plastics are attracting attention as a material to replace conventional plastics.[6–12] Biodegradable plastics and their derivative materials are broken down by microbes into water and CO_2 within a period of time.[13–17] Among the various biodegradable plastics, aliphatic polyester-based biodegradable plastics include poly(lactic acid) (PLA),[18–21] poly(hydroxyalkanoate) (PHA),[22–31] poly(glycolic acid) (PGA),[32–35] poly(caprolactone) (PCL),[36–40] poly(butylene succinate) (PBS),[41–44] poly(carbonate)[45–49] and so on, as shown in Fig. 1.

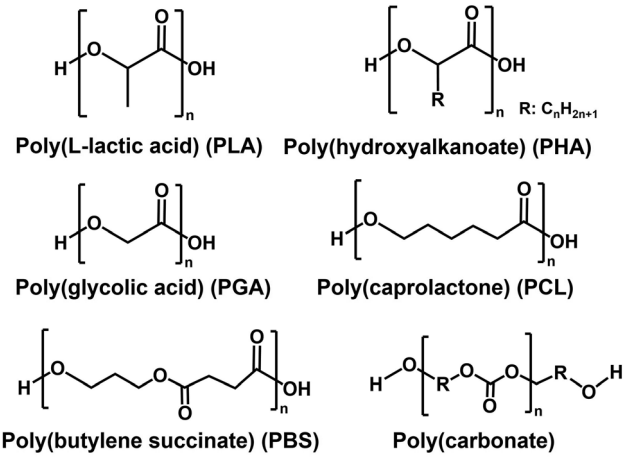

Fig. 1 Chemical structures of typical biodegradable plastics.

The precursors of these biodegradable plastics are synthesised from various molecules, such as biological and petroleum-derived molecules. Therefore, it is required to establish precursor synthesis methods from renewable raw materials such as CO_2 and biomass-derived molecules in the future. In natural photosynthesis, visible light energy is used as the driving force to produce glucose, starch, and oxygen using CO_2 and water as raw materials.[50–55] Thus, natural photosynthetic processes can serve as models for the CO_2-based synthesis of polymers and their precursors. Natural photosynthesis consists of light-dependent reactions and dark reactions. The main components involved in the light-dependent reactions are the photosystem, the complexes that capture light energy, chlorophyll, the main light-absorbing pigments, the electron transport chain that transports electrons and contributes to the production of adenosine triphosphate (ATP) and the reduced form of nicotinamide adenine dinucleotide phosphate (NADPH), ATP synthase and ferredoxin $NADP^+$ reductase. In summary, a light-dependent reaction is a process that converts absorbed visible-light energy into ATP and NADPH.

The dark reactions, collectively known as the Calvin cycle,[56,57] do not directly require visible-light energy but utilize the ATP and NADPH produced during the light-dependent reactions to fix CO_2 into organic compounds, such as ribulose-1,5-bisphosphate, and convert them into glucose through enzymatic processes. Biodegradable plastics and their precursors are synthesized starting from compounds synthesized from CO_2 produced in the Calvin cycle using microalgae. It has been reported that D-lactate, a precursor for poly(lactic acid), was produced using malic enzyme (ME)-overexpressing strains of cyanobacterium *Synechocystis* sp. PCC6803, as shown in Fig. 2.[58]

A metabolic map of the TCA cycle in *Synechocystis* sp. PCC 6803 is shown in Fig. 3.[59] As shown in Fig. 3, not only D-lactate but also various biodegradable plastic precursors, such as succinate, 3-hydroxybutyrate, and 3-hydroxypropionate, can be produced from CO_2 under visible-light irradiation using *Synechocystis* sp. PCC 6803. Additionally, poly(hydroxybutyrate) (PHB) is produced from CO_2 using *Synechocystis* sp. PCC 6803. The metabolic map in Fig. 3 shows that the production of acetyl Co-A from CO_2 leads to the production of various biodegradable plastic precursors. It will also be possible to produce biodegradable plastic precursors, such as fumarate and malate.

In this way, by linking the TCA cycle and glycolysis with the photosynthetic process, it is possible to synthesize biodegradable plastics and their precursors from CO_2 driven by light energy.

To develop a visible-light driven process for the production of CO_2-based biodegradable plastics and their precursors, based on the mechanisms of natural photosynthesis and microalgae, a method of linking light-driven redox (light-dependent reaction) with reactions mediated by biocatalytic

Yutaka Amao

Professor Yutaka Amao received his doctorate in Engineering in 1997 from the Tokyo Institute of Technology, Japan. He worked as a Researcher at the Kanagawa Academy of Science and Technology from 1997 to 1998, as a researcher at the National Aerospace Laboratory from 1998 to 2001, and as an Associate Professor in the Department of Applied Chemistry of Oita University from 2001 to 2013. He also worked as a Precursory Research for Embryonic Science and Technology (PRESTO) Researcher at the Japan Science and Technology Agency from 2011 to 2016. From 2013 to 2020, he was a Full Professor at the Advanced Research Institute for Natural Science and Technology, Osaka City University. In 2020, he was appointed as a Full Professor at the Research Centre for Artificial Photosynthesis, Osaka City University (now Osaka Metropolitan University after its merger with Osaka Prefecture University in 2022). He was appointed as a Fellow of the Royal Society of Chemistry in 2018. His current research interests ilude the development of photocatalysts, molecular catalysts, biocatalysts, and strategies for thecarbon dioxide conversion to organic molecules usinghybrid catalysis systems.

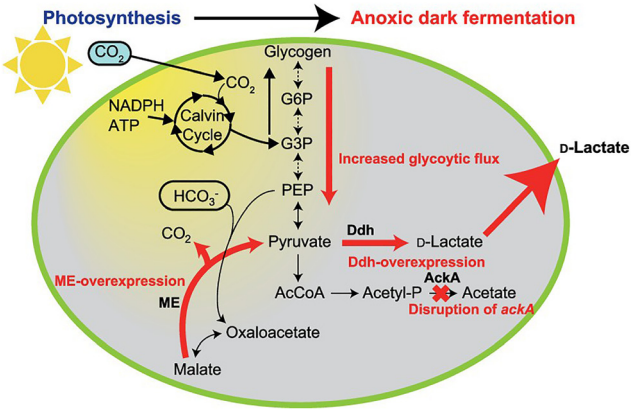

Fig. 2 Light-driven D-lactate production from CO_2 using *Synechocystis* sp. PCC6803. G6P: glucose-6-phosphate, G3P: glyceraldehyde 3-phosphate, PEP: phosphoenolpyruvic acid, ME: malic enzyme, Ddh: D-lactate dehydrogenase, AckA: acetate kinase A. Reproduced with permission from ref. 58. Copyright 2020, the American Chemical Society.

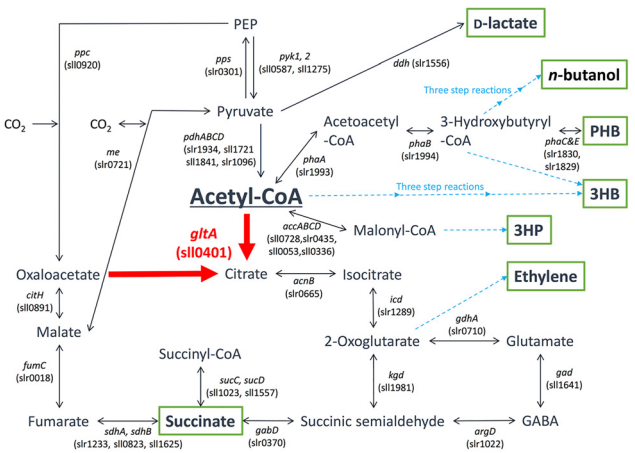

Fig. 3 Metabolic map of the TCA cycle in *Synechocystis* sp. PCC 6803. *accABCD*: acetyl-CoA carboxylase, *acnB*: aconitase, *argD*: D-arginine dehydrogenase, *citH*, malate dehydrogenase, *ddh*: D-lactate dehydrogenase, *fumC*: fumarase, *gabD*: succinate-semialdehyde dehydrogenase, *gad*: glutamate decarboxylase, *gdhA*: glutamate dehydrogenase, *gltA*: citrate synthase, *icd*: isocitrate dehydrogenase, *kgd*: 2-oxoglutarate decarboxylase, *me*: malic enzyme, *pdh*ABCD: pyruvate dehydrogenase, *phaA*: β-ketothiolase, *phaB*: acetoacetyl-CoA reductase, *phaC&E*: polyhydroxyalkane synthase, *ppc*: phosphoenolpyruvate carboxylase, *pps*: phosphoenolpyruvate synthase, *pyk*1, 2: pyruvate kinase, *sdhA*, *sdhB*: succinate dehydrogenase, *sucC*, *sucD*: succinate dehydrogenase. A. Reproduced with permission from ref. 59. Copyright 2019, The authors Creative Commons CC-BY-NC-ND license.

processes such as microbials or enzymes (dark reaction) has been envisaged, as shown in Fig. 4.

Using semiconductor photocatalysts and organic dyes in a light-driven redox system, light-harvesting and sensitizing functions can be enhanced compared to natural photosynthesis, such as that in microalgae. Biocatalytic processes use microorganisms directly or through cascades of enzymes to produce biodegradable plastics and their precursors from CO_2. By linking these two processes, it is expected that biodegradable

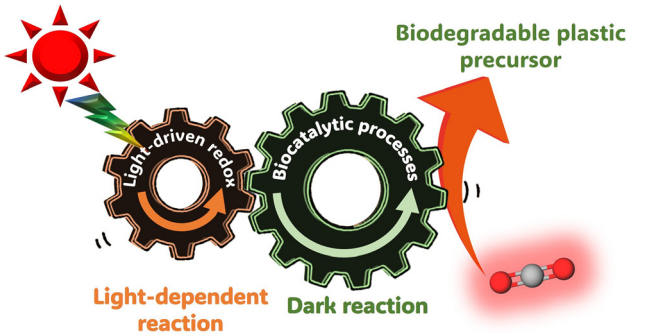

Fig. 4 CO_2-based biodegradable plastics and their precursor production using systems comprising visible-light-driven redox reactions and biocatalytic processes.

plastics and their precursors can be produced by fixing CO_2 to organic molecules using visible-light energy as a driving force.

In this review article, recent research on the visible-light-driven production of CO_2-based biodegradable plastics and their precursors with a system comprising light-driven redox and biocatalytic processes is introduced. First, research on the production of biodegradable plastics and their precursors using semiconductor photocatalysts as photoredox and microbials as biocatalytic processes is introduced. Second, research on the production of biodegradable plastic precursors using organic dye-based photoredox and enzyme-based biocatalytic processes is introduced.

Strategy for the visible-light-driven production of CO_2-based biodegradable plastics and their precursors with a photocatalyst and microbial cell hybrid system

Semiconductor-based photocatalysts are highly efficient at capturing and converting solar energy compared to the light-harvesting function of natural photosynthesis. Meanwhile, natural CO_2 fixation, primarily by plants and microorganisms, is the basis of life and biological processes. By directly contacting semiconductor-based photocatalysts with microbial cells expressing a CO_2 fixation pathway, as shown in Fig. 5(a), light-driven biodegradable plastics and their precursors can be produced. Additionally, a system for biodegradable plastics and their precursor production from CO_2 using microbial cells and extract containing enzymes as the biocatalyst in a visible light-driven redox system, consisting of an electron donor (ED), a visible light sensitizer (PS), and an electron mediator (EM), has been proposed, as shown in Fig. 5(b).

In the system shown in Fig. 5(a) and (b), a visible light-responsive photocatalyst capable of decomposing water into oxygen and hydrogen is used.[60–65] However, the CO_2 fixation pathway within microbial cells for the production of biodegradable plastics and their precursors is shown in Fig. 6. As shown in Fig. 6, natural CO_2 fixation pathways are classified into the following six categories: Calvin Benson Bassham (CBB) cycle,[66] 3-hydroxypropionate pathway,[67] reductive acetyl-CoA (Wood-Ljungdahl (WL) pathway) pathway,[68] reductive TCA cycle,[69] dicarboxylate/4-hydroxybutyrate cycle,[70] and 3-hydroxypropionate/4-hydroxybutyrate cycle.[71] In particular, the reductive acetyl-CoA

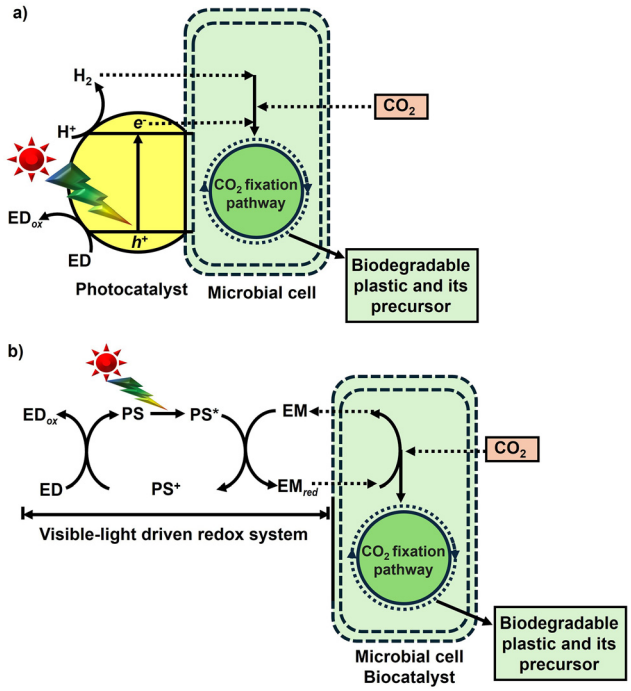

Fig. 5 Visible-light-driven production of biodegradable plastics and their precursors based on CO_2 fixation using a photocatalyst and microbial cell hybrid system (a) and a hybrid system of photoredox consisting of an electron donor (ED), a visible light sensitizer (PS), and an electron mediator (EM) and the microbial cells or biocatalysts (b).

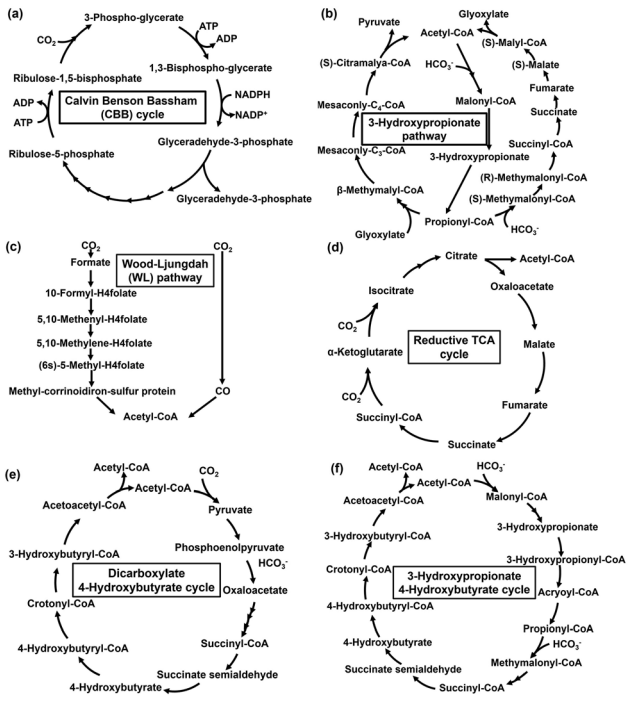

Fig. 6 Six natural CO_2 fixation pathways: (a) Calvin Benson Bassham (CBB) cycle. (b) 3-hydroxypropionate pathway. (c) Wood-Ljungdahl (WL) pathway. (d) Reductive TCA cycle. (e) Dicarboxylate/4-hydroxybutyrate cycle. (f) Hydroxypropionate/4-hydroxybutyrate cycle.

pathway, known as the Wood-Ljungdahl (WL) pathway, is expressed in *Moorella thermoacetica* (*M. thermoacetica*) and is used to produce acetate from CO_2[72–75] combined with a photocatalyst.

Visible-light-driven acetate production from CO_2 with a photocatalyst and microbial cell hybrid system

First, a production system for acetate, a precursor of biodegradable plastics, from CO_2 using a combination of photocatalysts is introduced.

Visible-light-driven acetate production from CO_2 using the hybridisation of CdS nanoparticles and *M. thermoacetica* has been accomplished. Fig. 7(A) shows a schematic representation

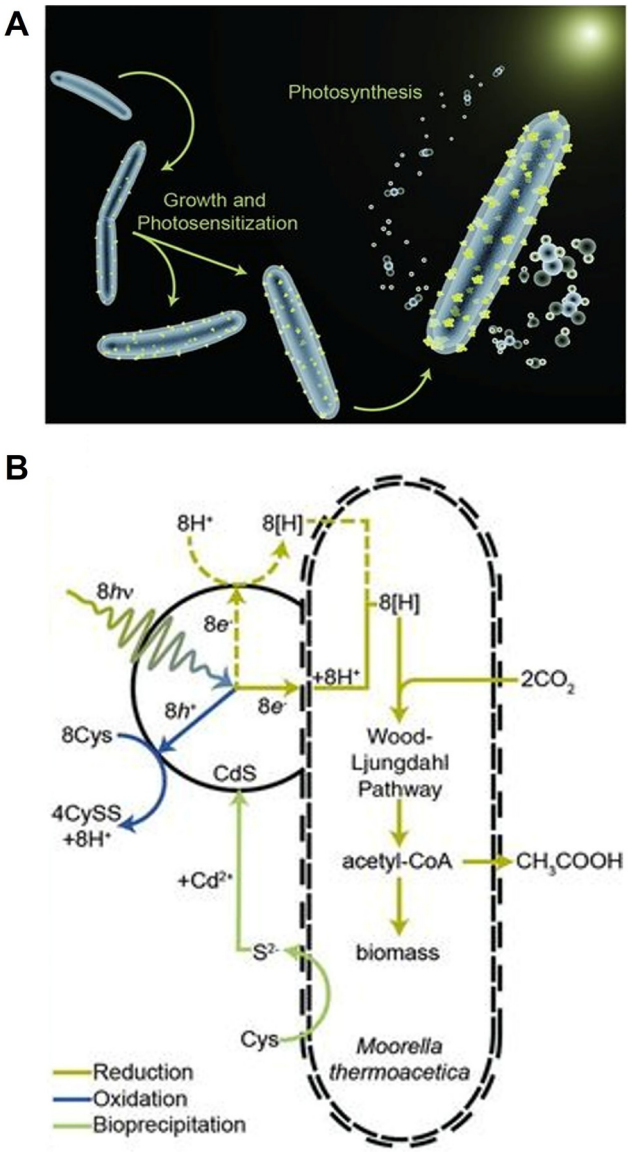

Fig. 7 Image of the visible-light-driven acetate production from CO_2 using a hybrid system comprising CdS nanoparticles and *M. thermoacetica* (A). Mechanism of visible-light-driven acetate production from CO_2 using CdS nanoparticles and *M. thermoacetica* in the presence of Cys (B). Reproduced with permission from ref. 76. Copyright 2016, the American Association for the Advancement of Science.

of acetate production from CO_2 using a hybrid system comprising CdS nanoparticles and *M. thermoacetica* (ATCC 39073) under visible-light irradiation.[76]

In this system, acetate can be produced from CO_2 using the photosensitizing function of CdS and the WL pathway in *M. thermoacetica*. In this system, CdS is constantly regenerated by incorporating cysteine (Cys) into the reaction. Visible-light-driven acetate production by *M. thermoacetica* and CdS is a two-step, one-pot synthesis, as shown in Fig. 7(B). First, CdS precipitation by *M. thermoacetica* is induced by adding Cd^{2+} and cysteine as sulfur sources.[77] *M. thermoacetica* performs acetate production using electrons generated from irradiated CdS nanoparticles, as shown in Fig. 7(B).

The Cys quenches h^+ of CdS, producing the oxidized disulfide form of cystine (CySS). Overall, this process is shown in Fig. 8.

Fig. 9 shows the time dependence of acetate production using a hybrid system of CdS–*M. thermoacetica* in the presence of Cys. The irradiation source is an in-house fabricated circular LED array composed of 405 ± 5 nm violet LEDs with a measured photon flux of 5.5×10^{18} cm^{-2} s^{-1}. As shown in Fig. 9, *ca.* 1.3 mM of acetate production is observed using a hybrid system of CdS–*M. thermoacetica* under visible-light irradiation. However, no acetate production is observed using *M. thermoacetica* under only visible-light irradiation. Moreover, no acetate production is observed using a hybrid system of CdS-sterilised *M. thermoacetica* under visible-light irradiation. Additionally, a decrease in the acetate concentration is observed under dark conditions. A maximum yield of *ca.* 90% acetate based on the initial Cys concentration is accomplished using a hybrid system of CdS–*M. thermoacetica* under visible-light irradiation. After 12 h of irradiation, 1.43 mM of acetate is produced.

Visible-light-driven acetate production using CO_2 as a raw material has also been reported using a hybrid system comprising gold nanoparticles (AuNPs) and *M. thermoacetica*.[78] Using this system, acetate production is estimated to be 6.01 mmol g^{-1} per week.

A tandem inorganic–biological hybrid system consisting of a TiO_2 nanoparticle loaded with a manganese(II) phthalocyanine (MnPc) cocatalyst, CdS and *M. thermoacetica* capable of oxygenic photosynthesis of acetate from CO_2 has been reported.[79] Fig. 10(A) shows a schematic representation of acetate production from CO_2 using a hybridisation system comprising CdS nanoparticles and *M. thermoacetica* under visible-light irradiation.

A feature of this system is that the photooxidation catalyst TiO_2 is loaded with the cocatalyst MnPc to regenerate the CySS/Cys redox shuttle, thereby coupling water oxidation with CySS reduction. Fig. 10(B) shows the time dependence of acetate production using the tandem system of TiO_2 nanoparticles loaded with MnPc, CdS and *M. thermoacetica* in the presence of Cys. The irradiation source is a filtered 75 W Xenon lamp (AM1.5G, 5% Sun).

$$2CO_2 + 8Cys \xrightarrow{h\nu} CH_3COOH + 2H_2O + 4CySS$$

Fig. 8 Overall process for the visible-light-driven acetate production from CO_2 using the hybrid system of CdS–*M. thermoacetica* in the presence of Cys.

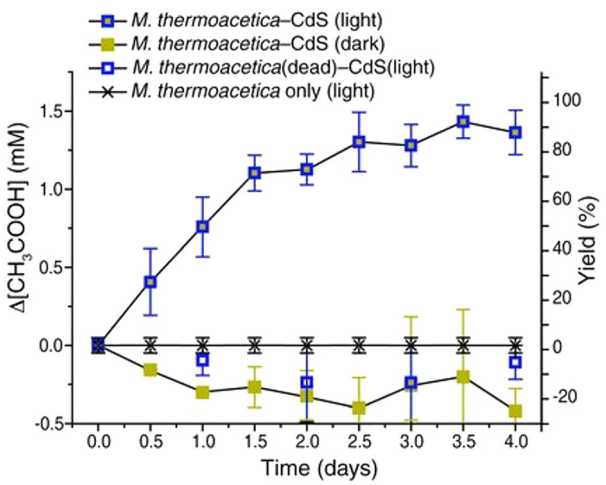

Fig. 9 Time dependence of acetate production from CO_2 using the hybrid system of CdS–*M. thermoacetica* in the presence of Cys under visible-light irradiation and dark conditions. Reproduced with permission from ref. 76. Copyright 2016, the American Association for the Advancement of Science.

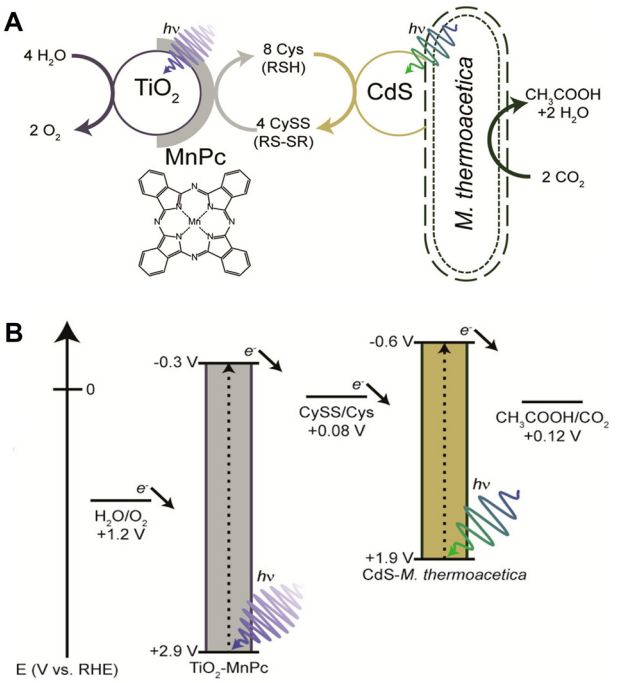

Fig. 10 Visible-light-driven acetate production from CO_2 using a hybrid system comprising TiO_2 nanoparticles loaded with MnPc, CdS nanoparticles and *M. thermoacetica* (A). Energy level diagram depicting the relative alignment of the energies of TiO_2 and CdS with the relevant redox processes (B). Reproduced with permission from ref. 79. Copyright 2016, American Chemical Society.

As shown in Fig. 11, comparing CdS–*M. thermoacetica* and MnPc-loaded TiO_2 to the control, the combined tandem system shows increased acetate production. Both CdS–*M. thermoacetica* alone and the MnPc-loaded TiO_2–*M. thermoacetica* control shows reduced acetate production below the stoichiometric limit imposed by Cys. Without MnPc, the TiO_2-only tandem system performed poorly. A comparison of the cumulative electron equivalents of acetate ($8e^-$) and O_2 ($4e^-$) measured over 3.5 days shows a strong correlation between the reduced product, acetate and the oxidized product, O_2. Using this system, 1.2 mM of acetate is produced after 1 day.

Visible-light-driven acetate production from CO_2 has been reported in which perylene diimide derivatives (PDI) and poly(fluorene-*co*-phenylene) (PFP) are applied to the *M. thermoacetica* surface as photosensitizers to form a p–n heterojunction (PFP/PDI) layer, as shown in Fig. 12(A).[80]

The accumulated acetate yield of PDI/PFP/*M. thermoacetica* (*ca.* 0.63 mM) is significantly higher than that of PDI/*M. thermoacetica* (*ca.* 0.25 mM) or PFP/*M. thermoacetica* (*ca.* 0.4 mM)

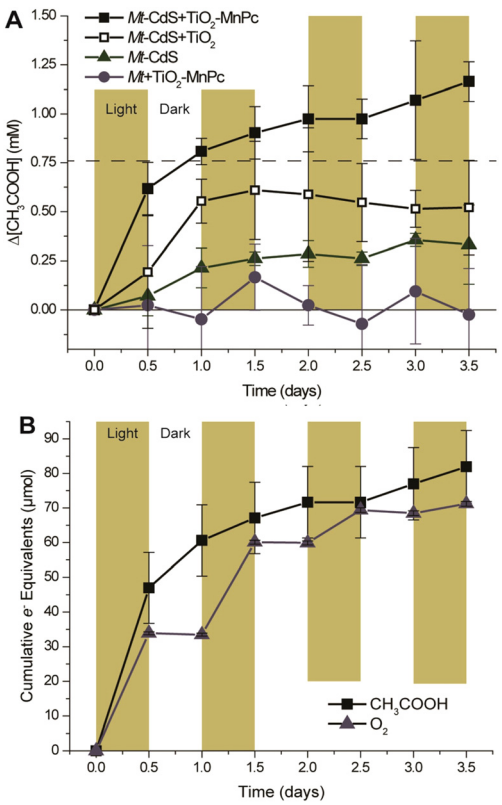

Fig. 11 Time dependence of acetate production from CO_2 with a tandem system comprising TiO_2 nanoparticles loaded with MnPc, CdS and *M. thermoacetica* in the presence of Cys under visible-light irradiation (■) (A). □: Tandem system comprising TiO_2 nanoparticles, CdS and *M. thermoacetica*, ▲: hybrid system comprising CdS and *M. thermoacetica*, ●: hybrid system of TiO_2 nanoparticles loaded with MnPc and *M. thermoacetica*. Time dependence of the amount of acetate and oxygen produced using a tandem system of TiO_2 nanoparticles loaded with MnPc, CdS and *M. thermoacetica* in the presence of Cys under visible-light irradiation (B). Reproduced with permission from ref. 79. Copyright 2016, the American Chemical Society.

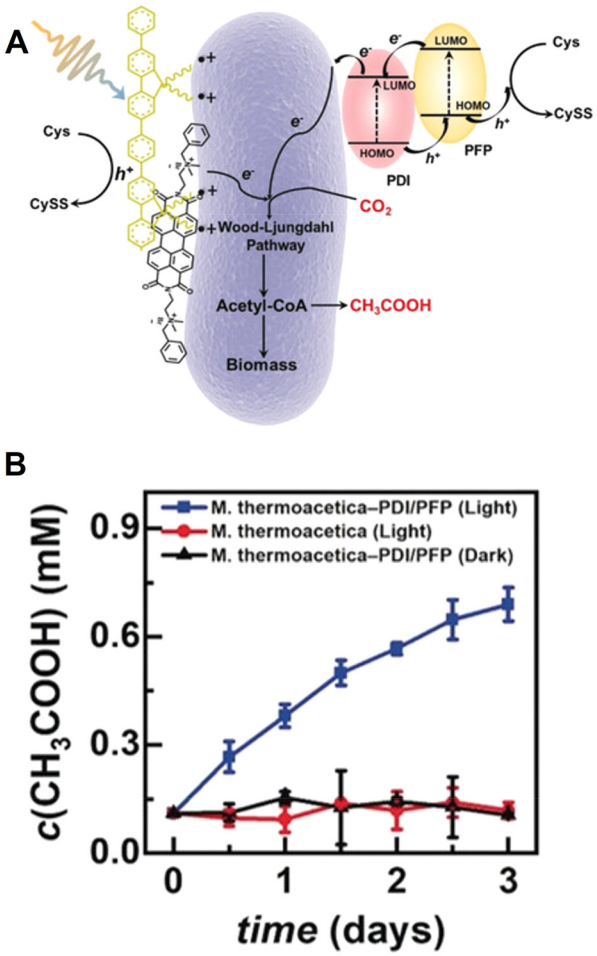

Fig. 12 Visible-light-driven acetate production from CO_2 using the PDI/PFP/*M. thermoacetica* hybrid system (A). Time-dependent acetate production from CO_2 with the PDI/PFP/*M. thermoacetica* hybrid system in the presence of Cys under visible-light irradiation (■). ■: Only *M. thermoacetica*, ▲: dark condition (B). Reproduced with permission from ref. 80. Copyright 2020 Wiley-VCH Verlag GmbH & Co. KGaA, Weinheim.

under irradiation using a Xenon fiber optic lamp with filters larger than 420 nm. Fig. 12(B) shows the time dependence of the acetate produced using PDI/PFP/*M. thermoacetica* in an alternating light–dark cycle of 12 h each.

After 3 days of incubation with irradiation, the accumulation amount of the acetate is estimated to be 0.63 mM. The quantum yield of 1.6% is calculated based on the initial Cys concentration. Here, the quantum yield is calculated using eqn (1) (n: number of electrons, C: total acetate concentration, V: total suspension volume, ϕ (cm^{-2} s^{-1}): photo flux, A: area of illumination, t: reaction time, and N_A: Avogadro's number). Acetate is produced by the 8-electron reduction of CO_2; therefore, the n value is 8.

$$\text{Quantum yield}\ (\%) = \frac{nCVN_A}{\phi tA} \times 100 \qquad (1)$$

where n: number of electrons, C: total acetate concentration, V: total suspension volume, ϕ (cm^{-2} s^{-1}): photo flux, A: area of

illumination (5 cm^2), t: reaction time, and N_A: Avogadro's number.

Sporomusa ovata (*S. ovata*) is a type of bacterium characterized by banana-shaped cells. *S. ovata* cells are strictly anaerobic, Gram-negative, spore-forming, straight or slightly curved rods that are motile by lateral flagella.[81] There has been much research on the electrosynthesis of energy-containing carbon chains using *S. ovata*.[82,83] *S. ovata* is a candidate biological catalyst that converts sunlight, water, and CO_2 into oxygen and liquid fuel or variable chemicals.

Visible-light-driven acetate production from CO_2 using the hybridisation of CdS nanoparticles and *S. ovata* (CdS–*S. ovata*) has also been accomplished. Fig. 13 (A) shows a schematic representation of acetate production from CO_2 using CdS–*S. ovata* under visible-light irradiation.[84]

In this system, photoelectrons are generated by CdS under light irradiation and transferred to *S. ovata* to achieve acetate production using CO_2 as a raw material *via* the WL pathway. In this system, it is found that formate is produced as an intermediate and then is rapidly converted to the final product, acetate. Fig. 13(B) shows the visible-light-driven acetate production using CdS–*S. ovata* after 1 day of light irradiation and the controls in the presence of Cys. The intensity of light (400 ± 5 nm) is estimated to be 0.20 mW cm^{-2}. Each experiment is pressurized with 2.0 atm, 80% N_2 and 20% CO_2. In this figure, Bio-CdS means CdS–*S. ovata*. As shown in Fig. 13(B), a high concentration of acetate is observed using CdS–*S. ovata* during visible-light irradiation in contrast to the other systems. Using CdS–*S. ovata*, the quantum yield reaches 16.8% ± 9%, and the active time of the system can last for 5 days. The quantum yield is also estimated using eqn (1).

Visible-light-driven acetate production from CO_2 by the hybridization of a Z-scheme semiconductor photocatalytic system with *S. ovata* has been reported, as shown in Fig. 14(A).[85] In this system, the Z-scheme consists of particulate semiconductors La and Rh co-doped $SrTiO_3$ ($SrTiO_3$: La, Rh) and Mo-doped $BiVO_4$ ($BiVO_4$: Mo). In this system, photocatalytic particles are immobilised onto a sheet.

Using the hybridization of a Z-scheme semiconductor photocatalytic system consisting of $SrTiO_3$: La, Rh and $BiVO_4$: Mo with *S. ovata*, *ca.* 40 and 80 μmol cm^{-2} of acetate and oxygen production are observed after 15 h with 1 sun (AM 1.5G, 100 mW cm^{-2}) irradiation, as shown in Fig. 14(B). A gas mixture of 80% N_2 and 20% CO_2 is used in this system. The solar energy to acetate efficiency is estimated to be 0.70% ± 0.04%, and the apparent quantum yield is calculated to be

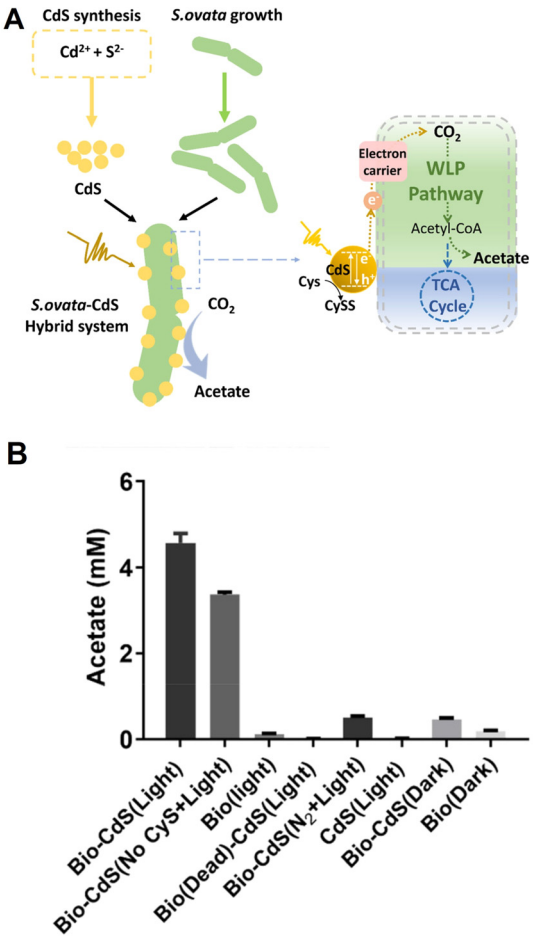

Fig. 13 Schematic of the visible-light-driven acetate production from CO_2 using CdS–*S. ovata* (A). Acetate production using CdS–*S. ovata* after 1 day of light irradiation in the presence of Cys. Bio-CdS (No CyS + Light): in the absence of Cys, Bio (light): only *S. ovata*, Bio(Dead)-CdS (Light): sterilized *S. ovata* and CdS hybrid system, Bio-CdS (N_2 + Light): without CO_2 gas, CdS (Light): only CdS. Dark: under dark conditions (B). Reproduced with permission from ref. 84. Copyright 2020, the American Chemical Society.

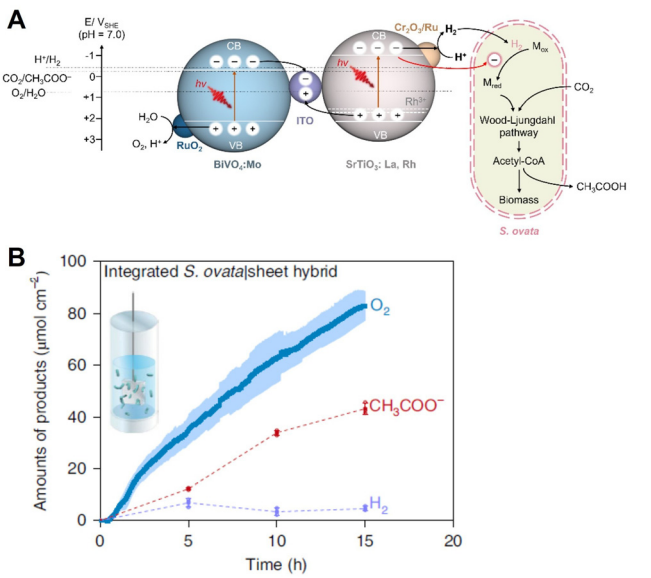

Fig. 14 Schematic of the visible light-driven acetate production from CO_2 by the hybridization of a Z-scheme semiconductor photocatalytic system consisting of $SrTiO_3$: La, Rh and $BiVO_4$: Mo with *S. ovata* (A). Time course of photosynthetic acetate, O_2 and H_2 production over *S. ovata*|Cr_2O_3/Ru-$SrTiO_3$:La,Rh|ITO|RuO_2-$BiVO_4$:Mo hybrids (B). Reproduced with permission from ref. 85. Copyright 2022, The Authors, under exclusive license to Springer Nature Limited.

21.3% at 420 ± 15 nm. The quantum yield is also estimated using eqn (1) in this experiment.

Visible-light-driven acetate production from CO_2 using a system that hybridises a semiconducting polymer with *S. ovata* is also studied.[86] The polymer semiconductor poly(3-hexylthiophene) (P3HT; chemical structure is shown in Fig. 15), widely used in the organic photovoltaic field,[87,88] is applied in this system.

Fig. 16 shows the schematic representation of visible-light-driven acetate production from CO_2 using a system of P3HT immobilised onto an indium tin oxide (ITO) coated glass substrate and *S. ovata* in the presence of Cys and an electron mediator (M).

Fig. 17 shows a schematic diagram of the exciton generation, separation, and transport processes in P3HT, [6,6]-phenyl-C_{61}-butyric acid methyl ester (P3HT: PCBM) heterojunction (bulk heterojunction (BHJ)), and a film with an ITO/ZnO/P3HT:PCBM/MoO_3 multilayer structure.

Here, visible-light-driven acetate production from CO_2 is investigated using a hybrid system comprising each P3HT-immobilised device and *S. ovata*. Cys and potassium ferricyanide are added as a hole-trapping agent and an electron mediator, respectively. The LED white light is used as an irradiation source with adjustable light intensity. A gas mixture

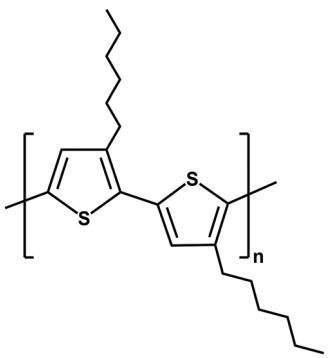

Fig. 15 Chemical structure of P3HT.

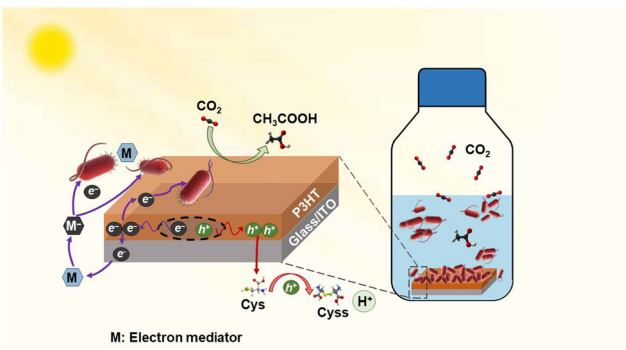

Fig. 16 Schematic of the visible light-driven acetate production from CO_2 using a system of PSHT immobilised ITO substrate with *S. ovata* in the presence of Cys and M. Reproduced with permission from ref. 86. Copyright 2024, the American Association for the Advancement of Science.

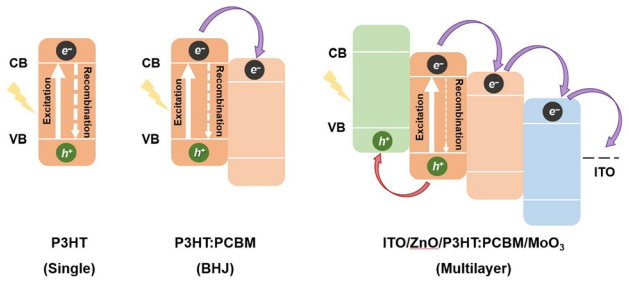

Fig. 17 Schematic of the exciton separation and recombination of polymer semiconductor films with P3HT, P3HT:PCBM bulk-heterojunction (BHJ), and multilayer film structures. CB, conduction band; VB, valence band. Reproduced with permission from ref. 86. Copyright 2024, the American Association for the Advancement of Science.

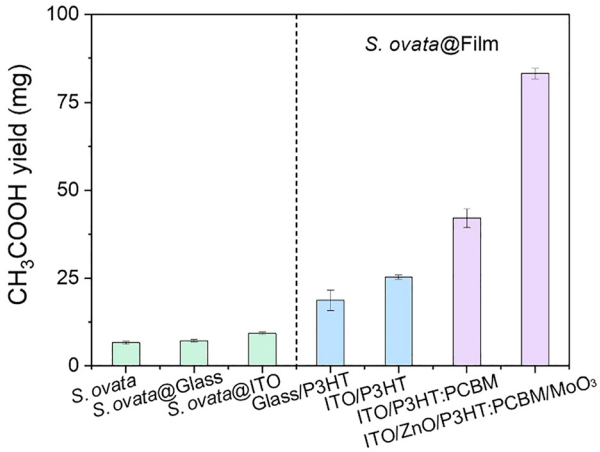

Fig. 18 Total acetate production using a hybrid system comprising a P3HT-immobilised device and *S. ovata* after 1 week of light irradiation in the presence of Cys and potassium ferricyanide. Reproduced with permission from ref. 86. Copyright 2024, the American Association for the Advancement of Science.

of 80% N_2 and 20% CO_2 is used as a carbon source in this system. Fig. 18 shows the total amount of acetate production from CO_2 using a hybrid system comprising each P3HT-immobilised device and *S. ovata*.

It is found that acetate production is improved using the hybrid system comprising ITO/ZnO/P3HT:PCBM/MoO_3 multilayer and *S. ovata* compared to other devices, as shown in Fig. 18. The quantum yield of the hybrid system comprising ITO/ZnO/P3HT:PCBM/MoO_3 multilayer and *S. ovata* reaches about 10%, which is obviously higher than 0.5% of the control system without a polymer semiconductor device. Additionally, in this experiment, the quantum yield is estimated using eqn (1).

Visible-light-driven acetate production from CO_2 using a system hybridising InP/ZnSe/ZnS quantum dots (QDs) with *S. ovata* in the presence of Cys and potassium ferricyanide is studied.[89] InP with a bandgap of 1.35 eV and a Bohr radius of approximately 10 nm can effectively absorb visible light.[90] Fig. 19(A) shows the schematic representation of visible-light-

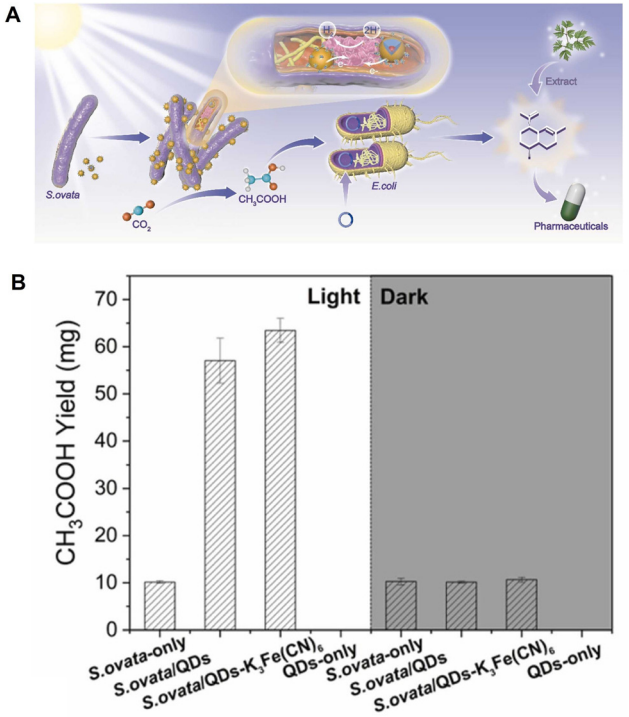

Fig. 19 Schematic of the visible light-driven acetate production from CO_2 using a hybrid system comprising InP/ZnSe/ZnS QDs and *S. ovata* (A). Total acetate production using the hybrid system comprising InP/ZnSe/ZnS QDs and *S. ovata* after 1 week of light irradiation in the presence of Cys and potassium ferricyanide (B). Reproduced with permission from ref. 89. Copyright 2022, Elsevier Ltd.

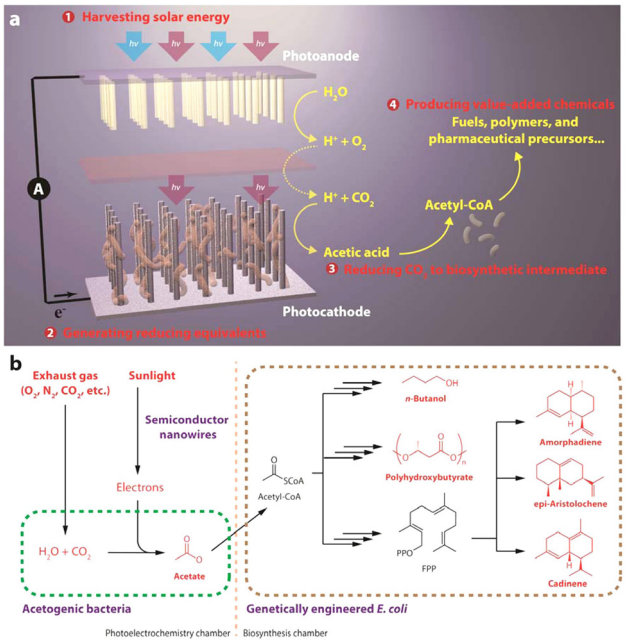

Fig. 20 Schematic of a photoelectrochemical cell consisting of silicon nanowire-integrated *S. ovata*: (a) Proposed approach for solar-powered CO_2 fixation includes four general steps: (1) harvesting solar energy, (2) generating reducing equivalents, (3) reducing CO_2 to biosynthetic intermediates, and (4) producing value-added chemicals. Through the integration of materials science and biology, such an approach combines the advantages of solid-state devices with living organisms. (b) As a proof of concept, under mild conditions, sunlight can provide the energy to directly treat exhaust gas and generate acetate as the biosynthetic intermediate, which can be upgraded into liquid fuels, biopolymers, and pharmaceutical precursors. FPP: farnesyl pyrophosphate. Reproduced with permission from ref. 94. Copyright 2015, American Chemical Society.

driven acetate production from CO_2 using a hybridising system of InP/ZnSe/ZnS QDs and *S. ovata*.

By growing a multilayer shell of ZnSe and ZnS on InP QDs synthesized using the hot injection method, the surface of the QDs can be passivated, and the stability of the InP QDs can be improved.[91,92] Furthermore, the low biotoxicity of InP QDs makes them potentially promising biological hybrid materials.[93]

In this system, Cys and potassium ferricyanide are also added as a hole-trapping agent and an electron mediator, respectively. The Xenon lamp with an AM 1.5 G filter is used as the irradiation source with adjusted light intensity. A gas mixture of 80% N_2 and 20% CO_2 is used as the carbon source in this system. Fig. 20(B) shows the total amount of acetate production from CO_2 using a hybridising system comprising InP/ZnSe/ZnS QDs and *S. ovata*. It is found that acetate production is improved using the hybridising system comprising InP/ZnSe/ZnS QDs and *S. ovata* in the presence of ferricyanide compared to other conditions, as shown in Fig. 20(B). The quantum yield of the hybridising system comprising InP/ZnSe/ZnS QDs and *S. ovata* in the presence of ferricyanide reaches about 7.0% estimated using eqn (1).

Visible-light-driven acetate production from CO_2 using a photoelectrochemical cell consisting of silicon nanowire integrated *S. ovata* as a photocathode has been reported, as shown in Fig. 20.[94]

Using a photoelectrochemical cell consisting of silicon nanowire integrated with *S. ovata*, visible-light acetate production is accomplished. Moreover, variable organic molecules are produced using a hybridisation system comprising engineered *E. coli* with this photoelectrochemical cell. In addition, it has been found that acetate production is improved using methanol-adapted *S. ovata* in this system.[95]

Visible-light-driven production of other plastic precursors from CO_2 using a photocatalyst and microbial cell hybrid system

Other plastic precursors that can be produced from CO_2 driven by visible light using a photocatalyst and microbial cell hybrid system are introduced.

Shikimic acid is a precursor for lignin production and can be a raw material for bioplastics.[96]

Visible-light-driven shikimic acid production using a system of polyphenol-functionalised indium phosphide (InP) with common heterotrophs, *Saccharomyces cerevisiae* (*S. cerevisiae*), has been reported, as shown in Fig. 21.[97] In this system, yeast strain *S. cerevisiae* Δzwf1 is selected. *S. cerevisiae* Δzwf1 is genetically engineered to overexpress four genes to enhance carbon flux through the shikimic acid pathway.[98]

Fig. 22 shows the specific shikimic acid production with the system using InP–*S. cerevisiae* Δzwf1 under visible-light

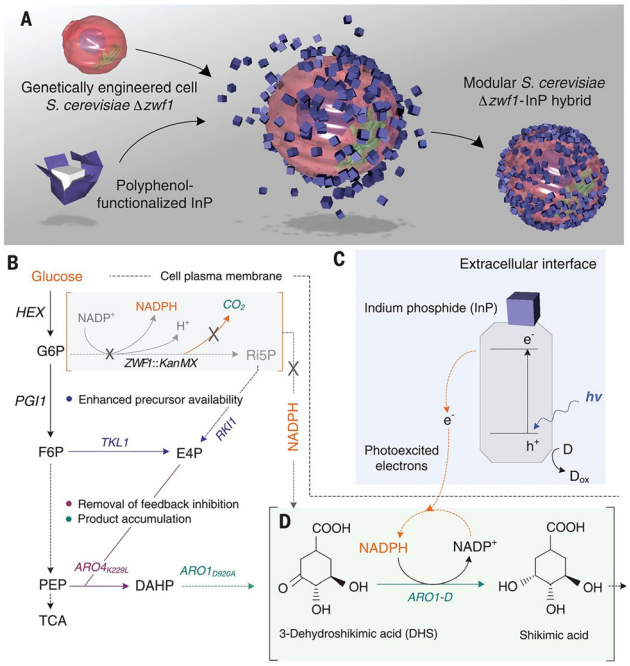

Fig. 21 Schematic of the preparation of InP–*S. cerevisiae* Δzwf1 (A). Metabolic engineering diagram for the overproduction of shikimic acid. *S. cerevisiae* Δzwf1 has the oxidative pentose phosphate pathway disrupted (ZWF1), leading to low cytosolic NADPH pools, which directly affect the shikimic acid pathway and reduce carbon loss in the production of CO_2 (B). Schematic of the cellular NADPH regeneration and shikimic acid biosynthesis assisted by photogenerated electrons from InP nanoparticles (C and D). G6P, glucose-6-phosphate; F6P, fructose-6-phosphate; Ri5P, ribulose-5-phosphate; E4P, erythrose-4-phosphate; PEP, phosphoenolpyruvate; DAHP, 3-deoxy-d-arabinoheptulosonate-7-phosphate; HEX, hexokinase; ZWF1, glucose-6-phosphate 1-dehydrogenase; PGI1, phosphoglucose isomerase; RKI1, ribose-5-phosphate ketol-isomerase; TKL1, transketolase; $ARO4_{K229L}$, feedback-insensitive DAHP synthase; $ARO1_{D920A}$, mutant pentafunctional aromatic enzyme; TCA, tricarboxylic acid cycle; *h*, Planck's constant; *ν*, frequency; h^+, electron hole; e^-, electron; *D*, putative electron donors in the cell culture medium; D_{ox}, oxidized electron donor species. Reproduced with permission from ref. 97. Copyright 2018, the American Association for the Advancement of Science.

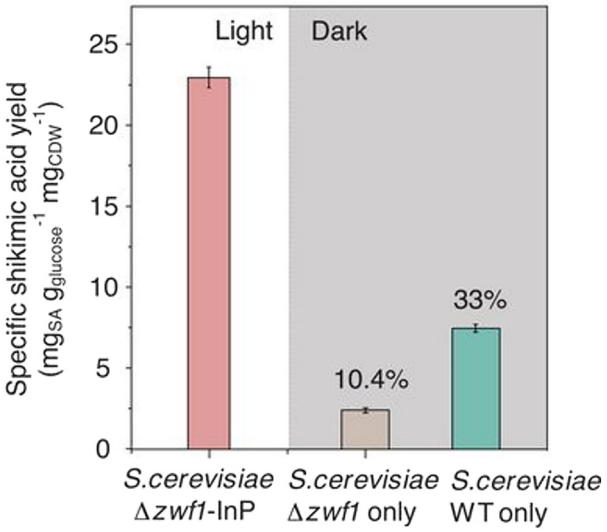

Fig. 22 Total shikimic acid production with InP–*S. cerevisiae* Δzwf1 under visible-light irradiation (5.6 mW cm^{-2}), with *S. cerevisiae* Δzwf1 or wild-type *S. cerevisiae* under the condition of dark incubation. Reproduced with permission from ref. 97. Copyright 2018, the American Association for the Advancement of Science.

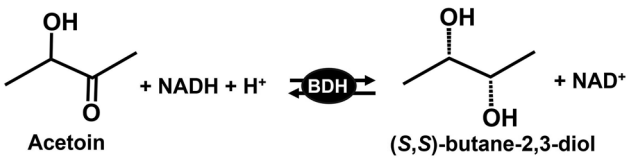

Fig. 23 BDH-catalysed (*S*,*S*)-butane-2,3-diol production from acetoin in the presence of NADH.

irradiation (5.6 mW cm^{-2}). The specific shikimic acid production with *S. cerevisiae* Δzwf1 or wild-type *S. cerevisiae* under the conditions of dark incubation is shown in Fig. 22. As shown in Fig. 22, the specific shikimic acid production increases using InP–*S. cerevisiae* Δzwf1 under visible-light irradiation compared with that of the system using *S. cerevisiae* Δzwf1 or wild-type *S. cerevisiae* under dark conditions.

3-Hydroxybutanone (acetoin) and 2,3-butanediol are two important four-carbon platform compounds with pharmaceutical and chemical synthesis applications.[99–102] (*S*,*S*)-Butane-2,3-diol is produced from acetoin in the presence of NADH with (S,S)-butanediol dehydrogenase (BDH; EC EC 1.1.1.76), as shown in Fig. 23.[103–105]

Visible-light-driven acetoin production from CO_2 with a hybrid system comprising eosin Y and *Ralstonia eutropha* (*R. eutropha*) has been reported.[106] *R. eutropha* has attracted significant research attention due to its excellent CO_2 fixation capacity and potential for expanding production diversity.[107] Fig. 24 shows the schematic representation of a hybrid system comprising eosin Y and *R. eutropha* for visible-light acetoin production from CO_2. In this system, eosin Y specifically binds to the membrane-bound hydrogenase (MBH) of *R. eutropha* and achieves targeted electron transfer to the hydrogenase-mediated electron transport and transformation pathway of

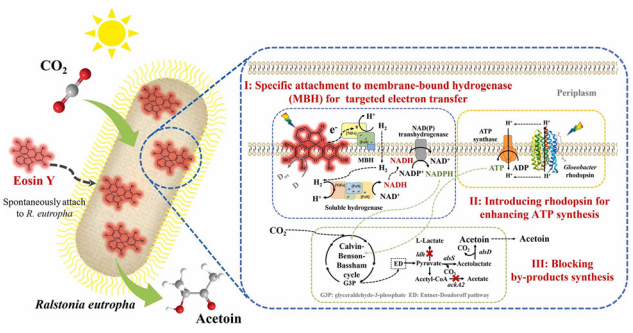

Fig. 24 Visible-light-driven acetoin production from CO_2 using a hybrid system comprising eosin Y and *R. eutropha*. Reproduced with permission from ref. 106. Copyright 2025, The Authors. Published by Elsevier Ltd. Creative Commons CC-BY license.

R. eutropha (pathway I). To enhance ATP synthesis, an oxygen-independent proton pump (*Gloeobacter rhodopsin*) is introduced into *R. eutropha* (pathway II). To promote carbon metabolic flux towards acetoin production, the by-product biosynthetic pathway is blocked (pathway III). The genetically engineered *R. eutropha* strain named REH01 is used in this system.

Fig. 25(A) shows the time dependence of acetoin production using a hybrid system comprising eosin Y and REH01 during visible-light irradiation using LED lamps (λ = 520 nm) with a certain light intensity (2, 5, or 10 mW cm^{-2}). Throughout the reaction, a gas mixture of CO_2/O_2 (molar ratio: 99/1) is continuously sparged into the reaction system. In this figure, biohybrid means a hybrid system comprising eosin Y and REH01.

As shown in Fig. 25(A), *ca.* 0.8 mM of acetoin production is observed after 24 h of irradiation. However, little acetoin production has been observed under other conditions. Furthermore, metabolic engineering strategies have been employed to enhance the acetoin-producing capability of REH01. REH01 strains lacking the GR and/or *ldh* and *ackA*2 genes have been prepared. Fig. 25(B) shows the time dependence of acetoin production with a hybrid system comprising eosin Y and genetically modified REH01 during visible-light irradiation. As shown in Fig. 25(B), the engineered eosin Y-GR expressing REH01 without the *ldh* and *ackA*2 biohybrid system achieves an acetoin yield of 1.41 ± 0.06 mM, which is 2.07 times larger than that of H_2-supplied autotrophic fermentation. Therefore, carbon flux can be directed towards acetoin production by inhibiting the L-lactate and acetate biosynthetic pathways.

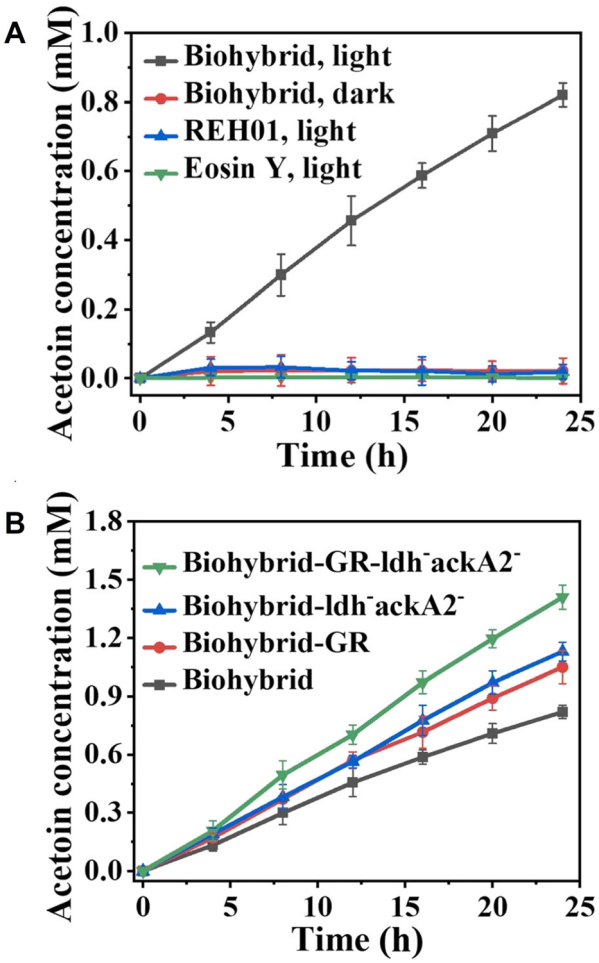

Fig. 25 Time-dependent acetoin production from CO_2 using a hybrid system comprising eosin Y and REH01 during visible-light irradiation. Red: dark condition, Blue: only REH01, Green: only eosin Y (A). Time dependence of acetoin production from CO_2 using a hybrid system comprising eosin Y and REH01 during visible-light irradiation. Green: eosin Y and GR expressing REH01 without *ldh* and *ackA*2. Bule: eosin Y and REH01 without *ldh* and *ackA*2. Red: eosin Y and GR expressing REH01. Black: eosin Y and REH01 (B). Reproduced with permission from ref. 106. Copyright 2025, The Authors. Published by Elsevier Ltd. Creative Commons CC-BY license.

Visible-light-driven polyhydroxybutyrate (PHB) production from CO_2 using a photocatalyst and microbial cell hybrid system

Among biodegradable plastics based on aliphatic polyesters, plastics derived from poly-3-hydroxybutyrate (PHB) are attractive because they are compostable, made from renewable feedstocks, and biodegradable.[108–115] The PHB can be produced from CO_2 driven by visible light using a photocatalyst and a microbial cell hybrid system. A hydrogen-oxidizing bacterium, *Ralstonia eutropha*, is used as a microbial cell for PHB production.[116]

The PHB production using an electrochemical system comprising cobalt-phosphorus (Co-P) alloy cathode and cobalt phosphate (CoP_i) anode with *Ralstonia eutropha* is reported for the first time.[117]

Visible-light-driven PHB production with a system comprising photocatalyst graphitic carbon nitride (g-C_3N_4) and *Ralstonia eutropha* H16 in the presence of triethanol amine (TEOA) is reported, as shown in Fig. 26(A).[118] As shown in Fig. 26(A), PHB is produced in *Ralstonia eutropha* H16 by utilizing the TCA cycle, Calvin–Benson–Bassham (CBB) cycle, NADH regeneration, and hydrogen.

Fig. 26(B) shows the total amount of PHB production using g-C_3N_4 and *Ralstonia eutropha* H16 in the presence of TEOA after 96 h of irradiation using an LED light set at 4200 lux. This figure also shows the amount of PHB produced in the absence of TEOA or g-C_3N_4. After 96 h irradiation, PHB production is improved 1.4 times to 6.73 ± 0.45 g l^{-1} with the system using g-C_3N_4 and *Ralstonia eutropha* H16 in the presence of TEOA. However, decreasing PHB production is observed using only *Ralstonia eutropha* H16 or without g-C_3N_4.

The development of a water-splitting enzymatic photocatalyst made of g-C_3N_4 coupled with H_2O_2-degrading catalase and its utilisation for a hybrid system with *Ralstonia eutropha* for visible-light-driven PHB production, as shown in Fig. 27(A).[119] Using catalase, it is possible to decompose hydrogen peroxide produced due to the two-electron oxidation of water into oxygen[120] by g-C_3N_4.[121]

Fig. 27(B) shows the total amount of PHB production using catalase-modified g-C_3N_4 and *Ralstonia eutropha* H16 after 48 h of irradiation using a 500 W Xe lamp with an AM1.5G filter.

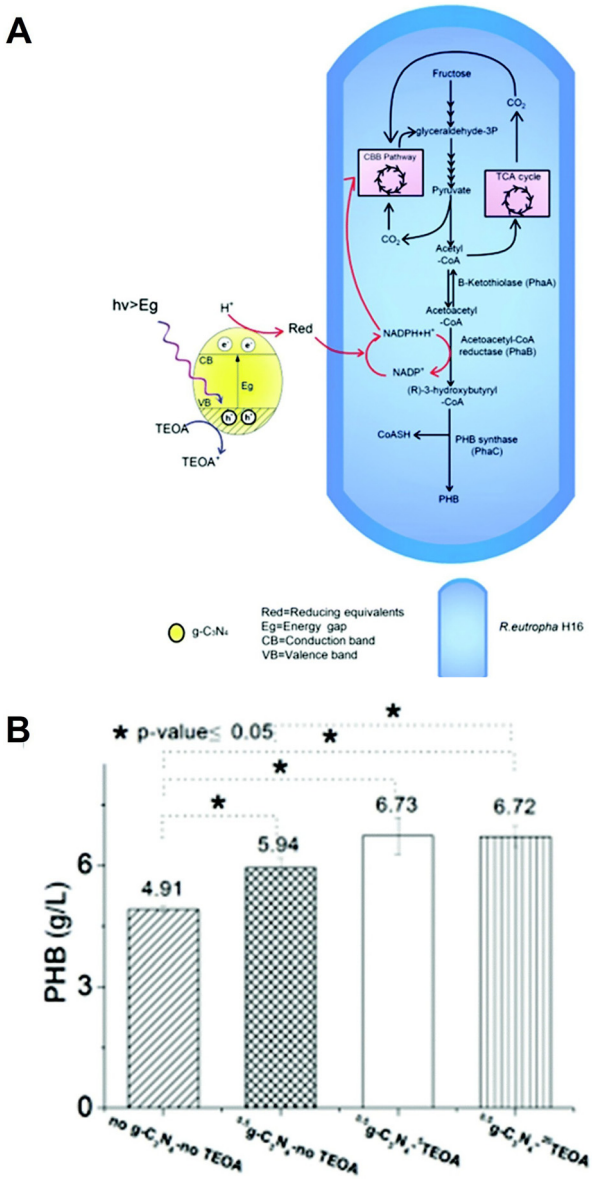

Fig. 26 Schematic of the visible-light-driven PHB production from CO_2 or fructose using a system comprising g-C_3N_4 and *Ralstonia eutropha* H16 in the presence of TEOA (A). Total PHB production using the system comprising g-C_3N_4 and *Ralstonia eutropha* H16 in the presence of TEOA after 96 h of irradiation with an LED light set at 4200 lux (B). Reproduced with permission from ref. 118. Copyright 2019, The Royal Society of Chemistry.

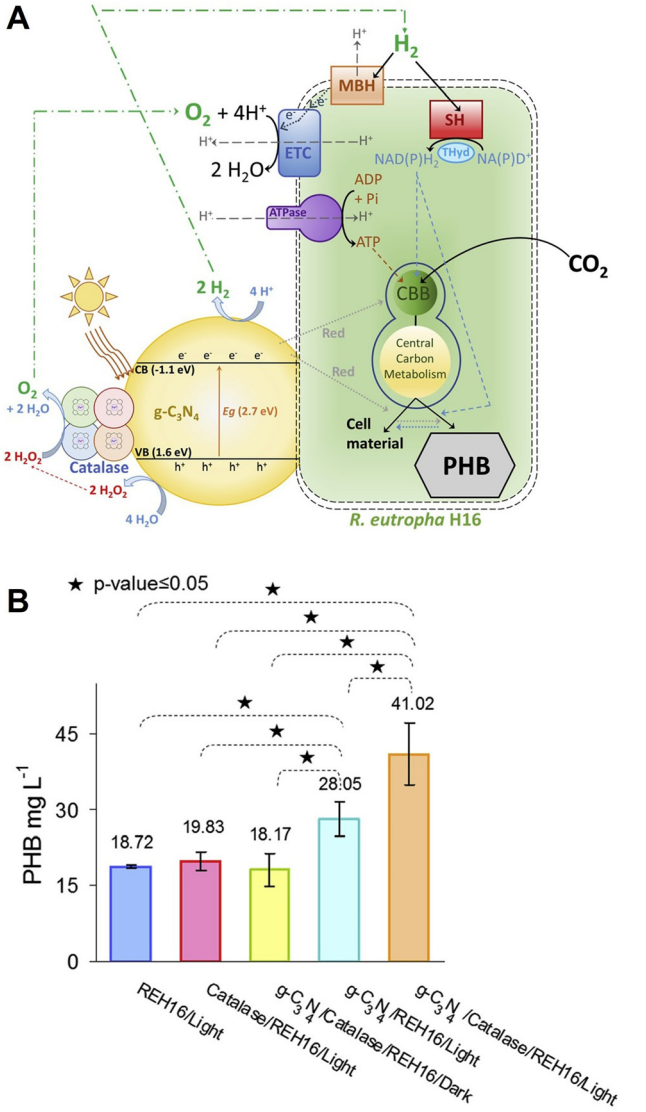

Fig. 27 Schematic of the visible-light-driven PHB production from CO_2 using a system comprising catalase-modified g-C_3N_4 and *Ralstonia eutropha* H16 (A). Total PHB production using the system comprising catalase-modified g-C_3N_4 and *Ralstonia eutropha* H16 after 48 h of irradiation using a 500 W Xe lamp with an AM1.5G filter (B). Reproduced with permission from ref. 119. Copyright 2020, The authors Creative Commons CC-BY-NC-ND license.

This figure also shows the amount of PHB produced using the system only *Ralstonia eutropha* H16, without g-C_3N_4, without catalase and under dark conditions.

The hybrid system built using the water-splitting g-C_3N_4-catalase photocatalyst doubles the production of the PHB by *Ralstonia eutropha* H16 from CO_2 and increases it by 1.84-fold from fructose. After 48 h of irradiation, *ca.*41 mg of PHB production is observed using catalase-modified g-C_3N_4 and *Ralstonia eutropha* H16 without any sacrificial electron donor reagent, such as TEOA.

Visible-light-driven PHB production from CO_2 using a system of conjugated polymer dots (Pdots) consisting of poly[*N*-9′-heptadecanyl-2,7-carbazole-*alt*-5,5-(4′,7′-di-2-thienyl-2′,1′,3′-benzothiadiazole)] (PFODTBT) and triblock copolymer ABA, poly(*N*,*N*-dimethylamino ethyl methacrylate)-*B*-poly(9,9-*N*-dihyxyl-2,7-fluorene)-*B*-poly(*N*,*N*-dimethylamino ethyl methacrylate) and PS-PEG-COOH (copolymer polystyrene grafted with carboxy-terminated polyethylene oxide) (PFODTBT Pdots)[122] and *Ralstonia eutropha* H16 (RH16/NR/Pdots) has been reported, as shown in Fig. 28(A) and (B).[123] In this system, Cys and neutral red (NR) are used as an electron donor and an electron mediator, as the example of Fig. 5(b). A Xenon fiber optic lamp with filters is employed using an AM 1.5G filter. The optimal

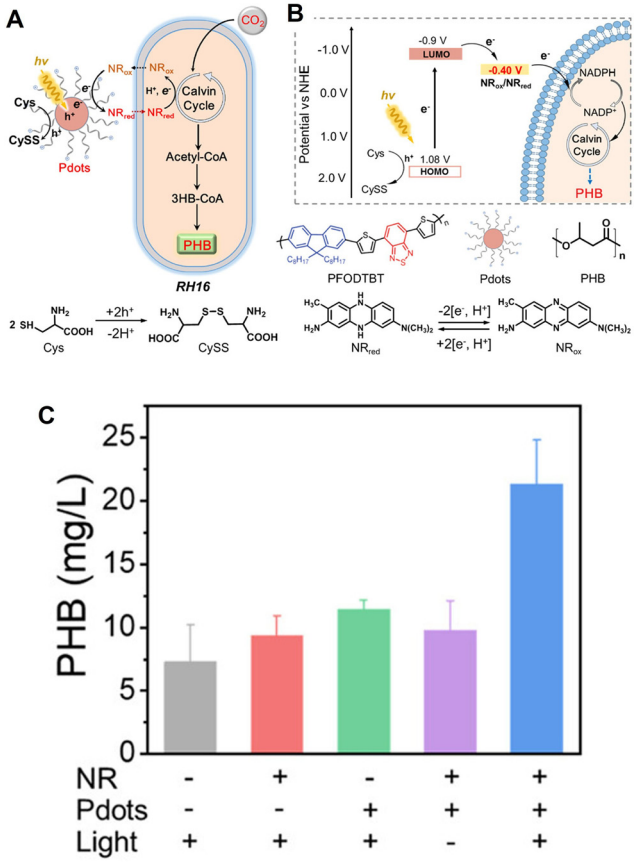

Fig. 28 Schematic of the visible-light-driven PHB production from CO_2 with RH16/NR/Pdots (A). Metabolic pathway of PHB production from CO_2 in RH16. 3HB-CoA: 3-hydroxybutyryl-CoA; PHB: polyhydroxybutyrate; h^+: electron hole; e^-: electron; Cys: cysteine; CySS: cystine; NR_{ox}: the oxidized state of NR; NR_{red}: the reduced state of NR (B). Schematic of Pdots promoting PHB production with RH16. Total PHB production using a system of RH16/NR/Pdots in the presence of Cys after 48 h of irradiation. "−" and "+" mean non-additive and added, respectively (C). Reproduced with permission from ref. 123. Copyright 2022, the American Chemical Society.

optical power density is determined to be 2.5 mW cm^{-2}. A gas mixture of 80% N_2 and 20% CO_2 is used as a carbon source in this system. Under light irradiation, the PHB production of RH16 is estimated to be only 7.3 ± 2.91 mg L^{-1} due to accumulation in the initial stage of autotrophic, as shown in Fig. 28(C).

The PHB productions of RH16/Pdots, RH16/NR, and RH16/NR/Pdots (under dark conditions) are estimated to be 9.3 ± 1.56, 11.4 ± 0.76, and 9.8 ± 2.35 mg L^{-1}, respectively.

As shown in Fig. 28(C), the production of PHB from the biohybrid system is slightly higher than that of RH16, suggesting that the addition of Pdots and NR is responsible for the increased amount of PHB in the solution. Under visible-light irradiation, the cumulative PHB production of RH16/NR/Pdots (21.3 ± 3.78 mg L^{-1}) increases significantly, which is an increase of 192% compared with only RH16. This is mainly because the visible-light-induced electrons of Pdots could be effectively transferred to the inside of RH16 by NR.

Visible-light-driven PHB production using a system comprising photocatalyst g-C_3N_4 and *Rhodopseudomonas palustris* (*R. palustris*)[124] in the presence of sulfur nanoparticles (SNPs) (g-C_3N_4–SNPs–*R. palustris*) is reported, as shown in Fig. 29(A).[125] In this system, SNPs act as dual electron donors, as shown in Fig. 29(A).

Fig. 29(B) shows the total PHB production using a system of g-C_3N_4–SNPs–*R. palustris* under irradiation with simulated daylight (~7000 lux) after 8 days. A gas mixture of 80% N_2 and 20% CO_2 is used as a carbon source in this system. Fig. 29(B) shows the PHB concentrations and percentage of cell dry weight occupied by PHB on day 8 (grey line).

The optimized g-C_3N_4–SNPs–*R. palustris* achieves a remarkable PHB production titer of 3.19 ± 0.03 g L^{-1} with 11.79% ± 0.93% quantum efficiency using solely CO_2 and SNPs.

A homogeneously autotrophic K/O co-doped g-C_3N_4 (K/O-CN) and *R. eutropha* biohybrid system is reported for visible-light-driven PHB production from CO_2, as shown in Fig. 30(A).[126] This system introduces nano-sized, scattered rod-like K/O co-doped g-C_3N_4 (K/O-CN) as a replacement for bulk g-C_3N_4,

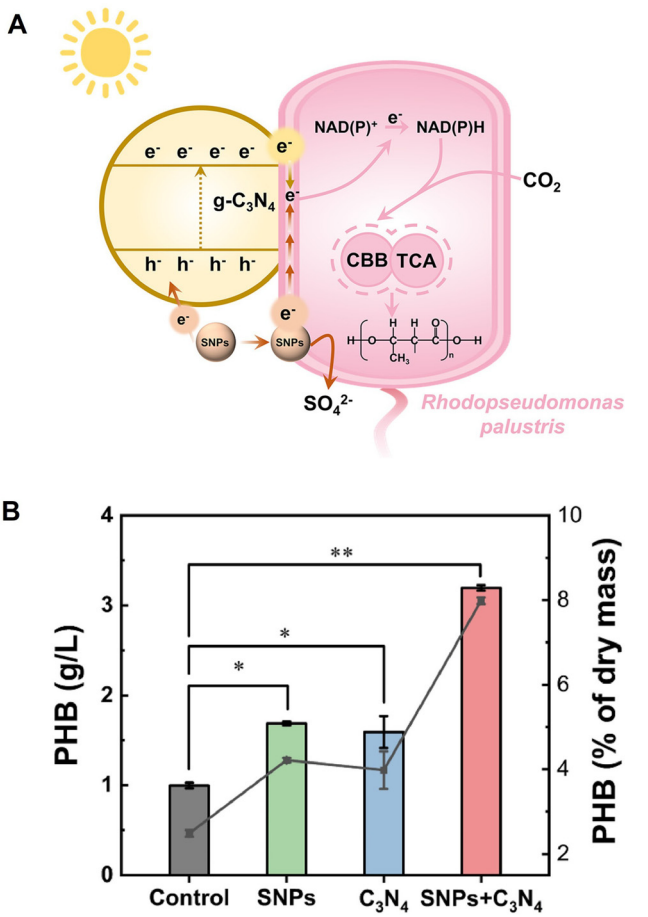

Fig. 29 Schematic of visible-light-driven PHB production from CO_2 using a system of g-C_3N_4–SNPs–*R. palustris* (A). Total PHB production from CO_2 using a system of g-C_3N_4–SNPs–*R. palustris* after 8 days of irradiation (B). Reproduced with permission from ref. 125. Copyright 2025, The Research Center for Eco-Environmental Sciences, the Chinese Academy of Sciences. Published by Elsevier B.V.

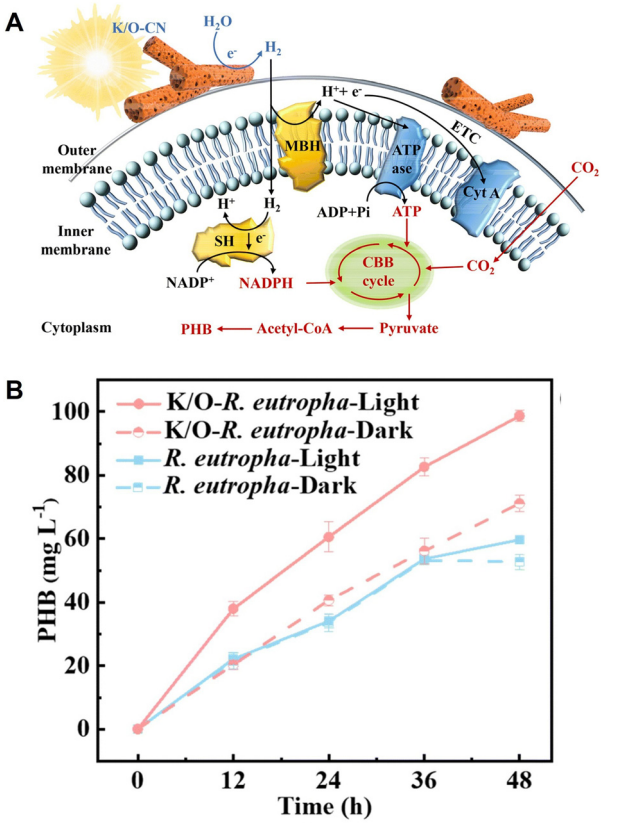

Fig. 30 Schematic of the visible-light-driven PHB production from CO_2 using a system of K/O-CN–*R. eutropha* (A). Time dependence of PHB production from CO_2 using the hybrid system of K/O-CN–*R. eutropha* under visible-light irradiation (B). Reproduced with permission from ref. 126. Copyright 2026, The Royal Society of Chemistry.

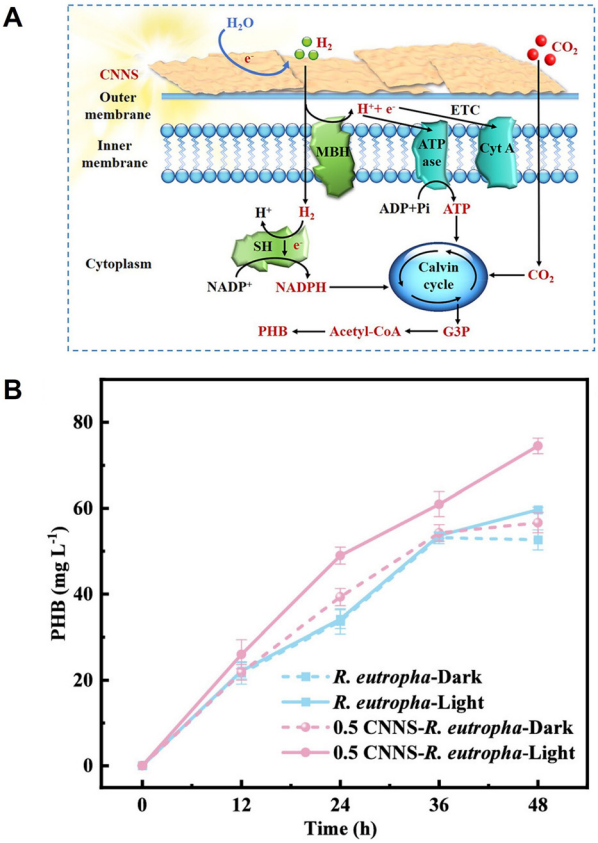

Fig. 31 Schematic of the visible-light-driven PHB production from CO_2 using a system of CNNS–*R. eutropha* (A). Time-dependent PHB production from CO_2 using the hybrid system of CNNS–*R. eutropha* under visible-light irradiation (B). Reproduced with permission from ref. 128. Copyright 2025, American Chemical Society.

therefore increasing the interface contact and mass transfer at the abiotic–biotic interface *R. eutropha*.

Fig. 30(B) shows the time dependence of PHB production using a system of K/O-CN–*R. eutropha* under visible-light irradiation with light at an intensity of 4000 lux (0.75 mW cm^{-2}). A gas mixture ($N_2:H_2:CO_2:O_2$ = 76 : 10 : 10 : 4) is used as a carbon source in this system. As shown in Fig. 30(B), the K/O-CN–*R. eutropha* biohybrid achieves a PHB yield of 49.35 ± 0.85 mg L^{-1} day^{-1}, surpassing non-metal-based biohybrids by adding co-factors and reaching a quantum efficiency of 5.88% ± 0.16%, which exceeds most metal-based biohybrid systems. Using K/O-CN–*R. eutropha*, the PHB production is improved compared to the dark condition or the system excluding K/O-CN.

A nanosheet composed of g-C_3N_4 is one of the promising visible light-responsive photocatalysts.[127] The g-C_3N_4 nanosheet (CNNS)–*R. eutropha* is reported for visible-light-driven PHB production from CO_2, as shown in Fig. 31(A).[128]

Fig. 31(B) shows the time dependence of PHB production using the CNNS–*R. eutropha* system under continuous irradiation at an intensity of 4000 lx. A gas mixture ($N_2:H_2:CO_2:O_2$ = 76 : 10 : 10 : 4) is used as a carbon source in this system. Comparative experiments are conducted under both light and dark conditions, as shown in Fig. 31(B). The CNNS–*R. eutropha* system exhibits the highest PHB yield of 37.25 ± 0.9 mg L^{-1} day^{-1} under irradiation with 0.5 g L^{-1} CNNS, demonstrating a 41.47% increase compared to the only *R. eutropha* under dark conditions (26.33 mg L^{-1} day^{-1}). Thus, the PHB production yield also surpasses the yields observed under both light and dark conditions without CNNS. Under dark conditions, the PHB yield is similar to whether CNNS is added. This result indicates that CNNS does not exert toxic effects on *R. eutropha* and that the enhancement in PHB production within this system is light-dependent.

We focus on the photocatalyst in a hybrid system comprising photocatalysts and microbial cells, as introduced in this section. The photocatalysts used in hybrid systems are visible-light-responsive semiconductors, and most of them have a proven track record in hydrogen production based on the photolysis of water. In hybrid systems, efficient electron and proton transfer from the photocatalyst to the microbial cell governs the CO_2 conversion rate. Therefore, developing catalysts that bring semiconductor photocatalysts into contact with the surface of microbial cells is crucial to achieving efficient CO_2 conversion.

Next, the separation of products based on CO_2 conversion using hybrid systems is discussed. Currently, the products from

the hybrid systems described in this section are separated only by high-performance liquid chromatography (HPLC). In addition, since microbial cells are used, suppressing by-products is another challenge for scaling up this system.

Visible-light-driven 3-hydoroxybutylate production from CO_2 and acetone with the photocatalytic dye and cell extract, including a multi-enzyme hybrid system

Another visible-light-driven production of biodegradable polymer precursor from CO_2 method is to use a cell extract containing crude enzymes, as shown in Fig. 32, instead of the microbial cell shown in Fig. 5(b).

This section describes the production of 3-hydroxybutyrate, a precursor of PHB, and a promising biodegradable plastic. The research example on visible-light-driven 3-hydroxybutyrate production with acetone carboxylase (AC; EC 6.4.1.6) and 3-hydroxybutyrate dehydrogenase (HBDH; EC 1.1.1.30) added as a catalyst in Fig. 32 is introduced. Fig. 33 shows the AC-catalysed acetoacetate production from acetone and bicarbonate in the presence of ATP (a) and HBDH-catalysed 3-hydroxybutyrate production based on the acetoacetate reduction in the presence of NADH (b). Using a dual-enzyme

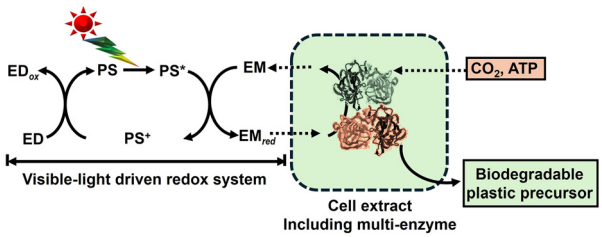

Fig. 32 Visible-light-driven production of biodegradable plastic precursors based on CO_2 fixation using a hybrid system of photoredox consisting of ED, PS, and EM and a cell-extract containing crude enzymes.

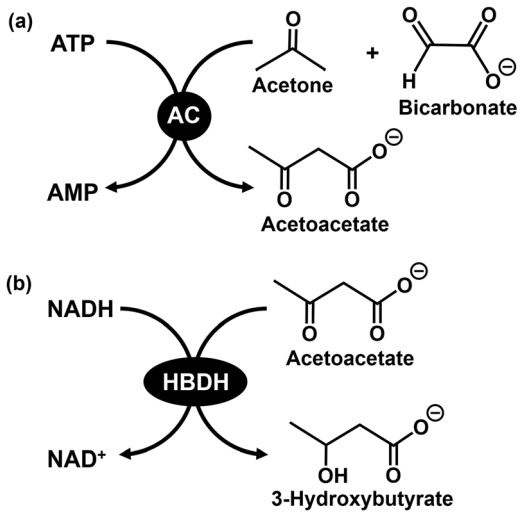

Fig. 33 AC-catalysed acetoacetate production from acetone and bicarbonate in the presence of ATP (a). HBDH-catalysed 3-hydroxybutyrate production based on the reduction of acetoacetate in the presence of NADH (b).

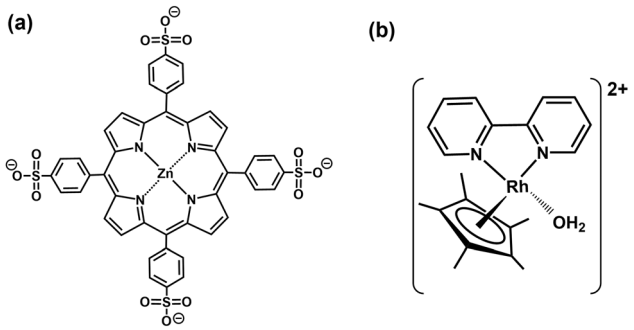

Fig. 34 Chemical structures of $ZnTPPS^{4-}$ (a) and $[RhCp^*(bpy)(H_2O)]^{2+}$ (b).

consisting of AC and HBDH, 3-hydroxybutyrate can be produced from acetone and bicarbonate *via* acetoacetate as an intermediate.[129,130]

Visible-light-driven 3-hydroxybutylate production from bicarbonate or CO_2 and acetone with a system comprising TEOA, zinc tetraphenylporphyrin tetrasulfonate ($ZnTPPS^{4-}$; chemical structure is shown in Fig. 34(a)), rhodium coordination complex ($[RhCp^*(bpy)(H_2O)]^{2+}$; Cp^* = pentamethylcyclopentadienyl, bpy = 2,2′-bipyridyl; chemical structure is shown in Fig. 34(b)), NAD^+, ATP, AC and HBDH is reported.[131,132]

AC[133,134] and HBDH[130] are expressed from photosynthetic bacteria *Rhodobacter capsulatus* SB1003 (*Rb. capsulatus* SB1003) cultured in acetone-bicarbonate medium. The cell extract containing AC and HBDH is obtained from *Rb. capsulatus* SB1003. First, visible-light-driven 3-hydroxybutyrate production from acetone and bicarbonate instead of CO_2 gas using a system comprising TEOA, $ZnTPPS^{4-}$, $[RhCp^*(bpy)(H_2O)]^{2+}$, NAD^+, ATP, and cell extract containing AC and HBDH is introduced.[131] After 5 h of irradiation using a 250 W halogen lamp ($\lambda >$ 390 nm), 379 μM of 3-hydroxybutyrate is produced in the sample solution of acetone (0.5 mM), TEOA (0.2 M), $ZnTPPS^{4-}$ (50 μM), $[RhCp^*(bpy)(H_2O)]^{2+}$ (5.0 μM), NAD^+ (2.0 mM), sodium bicarbonate (50 mM), sodium ATP (2.0 mM), magnesium chloride (5.0 mM) and cell extract (AC 0.051 U, HBDH 0.47 U) in 5.0 mL of 500 mM HEPES–NaOH buffer (pH 7.0). Using this system, the conversion yield of acetone to 3-hydroxybutyrate is approximately 76%.

Visible-light-driven 3-hydroxybutyrate production from acetone and directly captured CO_2 from a mixture of N_2 and CO_2 gases using the system comprising TEOA, $ZnTPPS^{4-}$, $[RhCp^*(bpy)(H_2O)]^{2+}$, NAD^+, ATP and enzyme extract containing AC and HBDH is introduced.[132] Fig. 35 shows the time dependence of acetoacetate (a) and 3-hydroxybutyrate (b) concentration in the sample solution of acetone (0.5 mM), TEOA (0.2 M), $ZnTPPS^{4-}$ (50 μM), $[RhCp^*(bpy)(H_2O)]^{2+}$ (5.0 μM), NAD^+ (2.0 mM), sodium ATP (2.0 mM), magnesium chloride (5.0 mM) and cell extract (AC 0.062 U, HBDH 0.7 U) in 5.0 mL of 500 mM HEPES–NaOH buffer (pH 7.0) under conditions with varying ratios of CO_2 and N_2 in the gas phase with irradiation using a 250 W Halogen lamp ($\lambda >$ 390 nm).

The results using this system are summarized in Table 1. The data in Table 1 are calculated from the figures published in ref. 132.

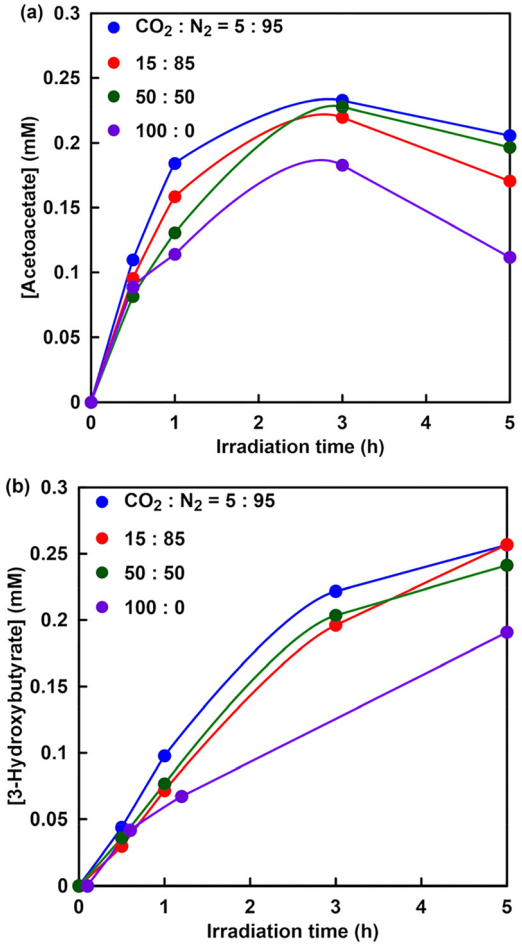

Fig. 35 Time-dependent concentration of acetoacetate (a) and 3-hydroxybutyrate (b) in the sample solution of acetone, TEOA, $ZnTPPS^{4-}$, $[RhCp^*(bpy)(H_2O)]^{2+}$, NAD^+, ATP, magnesium chloride and cell extract (AC, HBDH) in an HEPES–NaOH buffer (pH 7.0) under varying ratios of CO_2 and N_2 in the gas phase and irradiation. Reproduced with permission from ref. 132. Copyright 2023, The Royal Society of Chemistry.

As shown in Table 1, no significant difference in 3-hydroxybutyrate production is observed in the mixed gas with the ratio of CO_2 to N_2 not exceeding 0.5. In contrast, 3-hydroxybutyrate production decreases under conditions with 100% CO_2 gas compared to other conditions. This is because the reaction system is isochoric and CO_2 in the gas phase dissolves into the sample solution, leading to a decrease in pressure, as shown in Table 1. Under the condition of 100% CO_2, especially, it is predicted that the catalytic activity of cell extract involving AC and HBDH is inhibited based on the decrease in pressure in the reaction system during irradiation. Therefore, gaseous CO_2 can be directly used as a raw material without using bicarbonate because of the gas-phase low concentration gaseous CO_2 trapping function of the HEPES–NaOH buffer solution used in the reaction. In addition, the captured gaseous CO_2 is converted to bicarbonate in the HEPES–NaOH buffer and acts as a carboxylating agent for acetone with an enzyme extract, including AC. This suggests that several to 20% of the gaseous CO_2 contained in gases emitted from thermal power stations, steel mills and chemical plants[142] could be used as feedstock in this system.

Table 1 Concentration of 3-hydroxybutylate produced and conversion yield of acetone to 3-hydroxybutylate in the solution containing acetone, TEOA, $ZnTPPS^{4-}$, $[RhCp^*(bpy)(H_2O)]^{2+}$, NAD^+, ATP, magnesium chloride and cell extract containing AC and HBDH using a mixture gas with various ratios of CO_2 and N_2 ($[CO_2/N_2]$) after 5 h of visible light irradiation

$[CO_2]/[N_2]$	[3-Hydroxybutyrate] (μM) after 5 h of irradiation	Conversion yield for acetone to 3-hydoxybutyrate after 5 h of irradiation %
0	0	0
0.05	257	51.4
0.15	257	51.4
0.5	241	48.2
1.0	190	38.0

Finally, waste acetone and low-concentration CO_2 are used as raw materials in the visible-light-driven 3-hydroxybutyrate production with the system comprising TEOA, $ZnTPPS^{4-}$, $[RhCp^*(bpy)(H_2O)]^{2+}$, NAD^+, ATP and cell extract, including AC and HBDH.[132] Acetone is an abundant and useful chemical in the laboratory because it serves as a non-halogenated organic solvent that is miscible with water.[143] Acetone is relatively cheap, reasonably harmless and is often the solvent of choice in chemical laboratories for cleaning glassware contaminated with organic deposits. Although acetone is useful as a solvent, it also requires an efficient method for recycling after use. Because black permanent marker ink contains various organic solvents, such as *m*-xylene, iso-butanol, resin and oil soluble dyestuff, it can be used as a model for insoluble stains. The commercial black permanent marker ink used in this experiment contains 58% *m*-xylene, 14% iso-butanol, 16% resin and 12% oil soluble dyestuff. Here, black permanent marker ink dissolved in acetone is used as a waste solvent model. After adding the waste acetone to the HEPES–NaOH buffer, the supernatant is separated from the precipitate, and the supernatant, including acetone, *m*-xylene and iso-butanol, is used for the visible-light-driven 3-hydroxybutyrate production. The reaction mixture consists of supernatant, including acetone (0.5 mM), sodium ATP (2.0 mM), magnesium chloride (5.0 mM), TEOA (0.2 M), $ZnTPPS^{4-}$ (50 μM), $[RhCp^*(bpy)(H_2O)]^{2+}$ (5.0 μM), NAD^+ (2.0 mM) and cell extract (AC: 0.062 U and HBDH: 0.7 U), with a mixed gas of a CO_2 to N_2 ratio of 0.15 in 5 mL of 500 mM HEPES–NaOH buffer. Fig. 36 shows the time dependence of acetoacetate and 3-hydroxybutyrate concentrations in the sample solution during irradiation using a 250 W halogen lamp ($\lambda > 390$ nm).

After 5 h of irradiation, 0.28 mM of 3-hydroxybutyrate is produced. No significant difference is observed between pure and waste acetone in the visible-light-driven 3-hydroxybutyrate synthesis using low concentrations of gaseous CO_2.

Strategy for the visible-light-driven production of CO_2-based biodegradable plastic precursors using a photocatalytic dye and multi-enzyme hybrid system

The method of directly using microbial cells as a biocatalyst has the advantages of being simple and high in product yield, but it

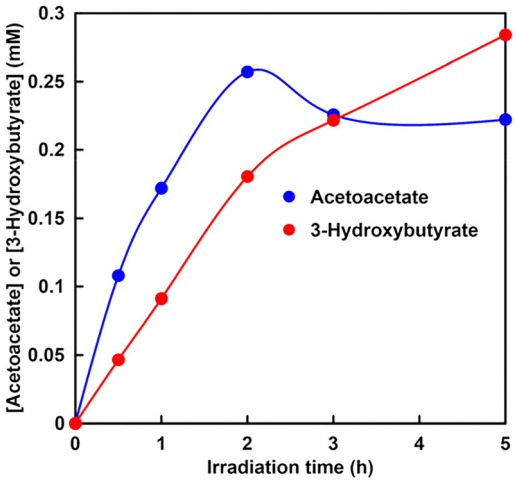

Fig. 36 Time-dependent concentration of acetoacetate or 3-hydroxybutyrate in the solution of the supernatant containing acetone, ATP, magnesium chloride, TEOA, $ZnTPPS^{4-}$, $[RhCp^*(bpy)(H_2O)]^{2+}$, NAD^+ and the cell extract (AC and HBDH:) in an HEPES–NaOH buffer in the presence of a gas mixture of a CO_2 to N_2 ratio of 0.15 in the gas phase under irradiation. Reproduced with permission from ref. 132. Copyright 2023, The Royal Society of Chemistry.

also has the drawback of difficulty in controlling the selectivity of the target product. Therefore, it has been proposed to produce biodegradable plastic precursors by incorporating an enzyme (ENZ) with the function of CO_2 fixation into a photoredox system consisting of an electron donor (ED), a visible light sensitizer (PS), and an electron mediator (EM), as shown in Fig. 37.[135–137]

By incorporating hydrogenase (H_2ase; EC 1.12.2.1; cytochrome-c_3 hydrogenase,[138–144] EC 1.12.7.2; ferredoxin hydrogenase[145–150]) and formate dehydrogenase[151–155] (FDH; EC 1.17.1.9; NAD^+-dependent, EC 1.17.1.10; $NADP^+$-dependent, and EC 1.17.98.4; selenium-containing formate dehydrogenase H) into a photoredox system consisting of ED, PS, and EM, visible-light-driven hydrogen production and formate production based on CO_2 reduction are achieved.

The first example of applying this system to the fixation of CO_2 to a substrate is shown in Fig. 38.[156]

In this system, $[Ru(bpy)_3]^{2+}$ (chemical structure is shown in Fig. 39) is used as the PS.

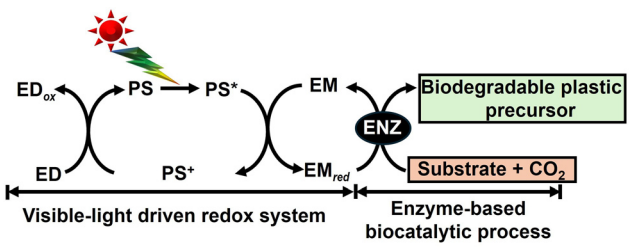

Fig. 37 Visible-light-driven production of biodegradable plastic precursors based on CO_2 fixation to a substrate using a system comprising an electron donor (ED), a visible-light sensitizer (PS), an electron mediator (EM) and an enzyme (ENZ).

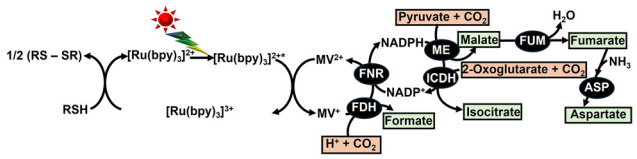

Fig. 38 Visible-light-driven CO_2 fixation using a photoredox system comprising 2-mercaptoethanol (RSH), tris(2,2′-bipyridyl)ruthenium(II) ($[Ru(bpy)_3]^{2+}$) and methyl viologen (MV^{2+})-linked enzymes. FNR: ferredoxin-$NADP^+$ reductase, ICDH: isocitrate dehydrogenase, FUM: fumarase, ASP: L-aspartase.

As shown in Fig. 38, FDH (EC 1.12.2.1), ICDH (EC 1.1.1.42), and ME (EC 1.1.1.40) can be used as CO_2 conversion enzymes in the photoredox system. When FDH is used as the enzyme in a photoredox system, the MV^+ can be used directly as a coenzyme instead of NAD(P)H. However, when ICDH or ME is used as an enzyme in a photoredox system, it is necessary to incorporate NADPH regeneration. As depicted in Fig. 38, biodegradable plastic precursors malate, fumarate, and aspartate are produced from CO_2 as a raw material using a photoredox system incorporating enzymes. Polymers derived from malate or aspartate precursors are biodegradable, as shown in Fig. 40.

Fumarate can also be used as a precursor to biodegradable plastic PBS. For the first time, a system incorporating ME, FUM (EC 4.2.1.2), and ASP (EC 4.3.1.1) as catalysts in a photoredox system comprising RSH, $[Ru(bpy)_3]^{2+}$, MV^{2+}, FNR (EC 1.18.1.2) and $NADP^+$ is successfully used to produce fumarate and aspartate from CO_2 and pyruvate under visible-light irradiation. Fig. 41 shows the time dependence of fumarate (a) and aspartate (b) production with a system comprising RSH (16 mM), $[Ru(bpy)_3]^{2+}$ (23 μM), MV^{2+} (0.16 mM), $NADP^+$(0.32 mM), pyruvic acid (40 mM), sodium bicarbonate (0.16 M), ammonium ion

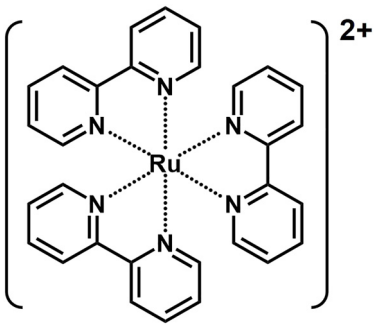

Fig. 39 Chemical structure of tris(2,2′-bipyridyl)ruthenium(II) ($[Ru(bpy)_3]^{2+}$).

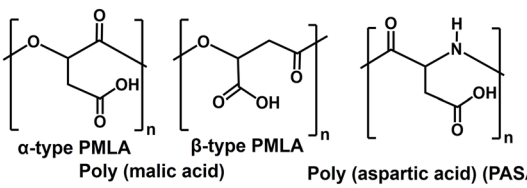

Fig. 40 Chemical structures of poly (malic acid)[157–159] and poly (aspartic acid).[160,161]

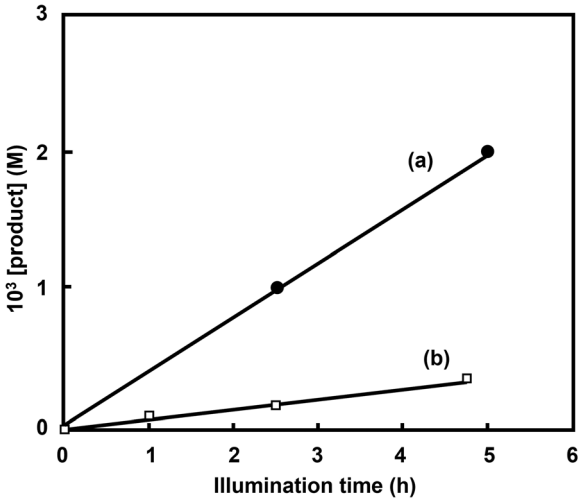

Fig. 41 Time-dependent concentration of aspartate (a) and fumarate (b) in a system comprising RSH, $[Ru(bpy)_3]^{2+}$, MV^2, $NADP^+$, pyruvic acid, sodium bicarbonate, ammonium ion, manganese chloride, FNR, ME, FUM and ASP in Tris-buffer solution during visible-light irradiation. Reproduced with permission from ref. 156. Copyright 1988, The Royal Society of Chemistry.

(80 mM), manganese chloride (80 μM), FNR (0.5 U), ME (0.5 U), FUM (156 U) and ASP (3.0 U) in 4.0 mL of 0.16 M Tris-buffer solution (pH 7.9) during visible-light irradiation (1000 W halogen quartz lamp with 400 nm cut-off filter).

As shown in Fig. 41, fumarate and aspartate production increase during visible-light irradiation. After 5 h of irradiation, *ca.* 1.3 and 2.0 mM of fumarate and aspartate are produced. In the absence of ASP, no aspartate is produced and malate and fumarate are produced during visible-light irradiation. Additionally, visible-light-driven malate production with the system comprising RSH (19 mM), $[Ru(bpy)_3]^{2+}$ (21 μM), MV^{2+} (0.19 mM), $NADP^+$(0.18 mM), pyruvic acid (47 mM), sodium bicarbonate (0.20 M), manganese chloride (95 μM), FNR (0.2 U) and ME (1.33 U) in 4.2 mL of 0.20 M Tris-buffer solution (pH 7.9) under a gaseous atmosphere of CO_2 during visible-light irradiation (1000 W halogen quartz lamp with 400 nm cut-off filter). After 2 h of irradiation, 3.0 mM of malate production is observed.[156]

Thus, in order to produce biodegradable plastic precursors, such as malate, fumarate, and aspartate, it is essential to develop a visible-light-driven NAD(P)H regeneration system consisting of ED, PS, EM, and a catalyst that can be linked to an enzyme-based biocatalytic process. Visible-light-driven NAD(P)H regeneration, consisting of ED, PS, EM, and a catalyst, has been extensively studied in two main systems (Fig. 42).[135–137] The first is a visible-light-driven NADPH regeneration system using FNR as a catalyst (Fig. 42(a)). The other is a visible-light-driven NAD(P)H regeneration system using $[RhCp^*(bpy)(H_2O)]^{2+}$ as a catalyst (Fig. 42(b)). In the system shown in Fig. 42(a), visible-light-driven NADPH regeneration systems using $[Ru(bpy)_3]^{2+}$,[156] 5-deazariboflavin,[162] riboflavin,[162] proflavin,[161,162] oligothiophene derivatives,[164] CdS,[165] CdSe quantum dots[166] and polyethylene glycol-modified chlorophyll-*a* (PEG-Chl-*a*)[167] as PSs are

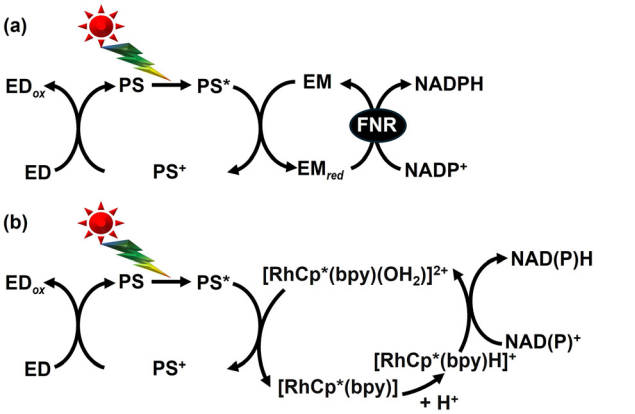

Fig. 42 Visible-light-driven NAD(P)H regeneration using a system comprising ED, PS, EM and FNR (a) and ED, PS, and $[RhCp^*(bpy)(H_2O)]^{2+}$ (b).

reported. In addition to 4,4′-bipyridinium salts, such as MV^{2+}, 2,2′-bipyridinium salts and ferredoxin are used as EMs in this system.[163] As shown in the system of Fig. 42(b), however, visible-light-driven NAD(P)H regeneration systems using carbon-doped TiO_2,[168] phosphate-doped TiO_2,[169] eosin-Y,[170] porphyrin derivatives[171,172] and proflavine[173] as PSs are reported. Research examples on visible light-driven NAD(P)H regeneration systems are summarized and reported in several reviews.[135–137,174,175]

The strategy for visible-light-driven CO_2-based biodegradable plastic precursor production using a photocatalytic dye and multi-enzyme hybrid system involves the integrated coupling of an NAD(P)H regeneration system and an enzyme-based biocatalytic process.

Visible-light-driven malate production using a photocatalytic dye and enzyme hybrid system

As mentioned above, visible-light-driven malate production from CO_2 and pyruvate using a system comprising RSH, $[Ru(bpy)_3]^{2+}$, MV^{2+}, $NADP^+$, FNR and ME has been developed for the first time. Some studies have been reported on the production of malate using visible light-driven NADPH regeneration catalysed by FNR in the presence of ME.

Visible-light-driven malate production from CO_2 and pyruvic acid (2.0 mM) using the system comprising RSH (27 mM), CdS or TiO_2 microcrystals fixed in the interlayer spacings of sodium montmorillonite (TiO_2/clay) (1.25 mM) as a PS, MV^{2+} (1.0 mM), $NADP^+$ (0.1 mM), FNR (0.2 U) and ME (1.0 U) in CO_2-saturated Tris-buffer (10 mL) has been reported.[175] For the system using CdS or TiO_2/clay, *ca.* 1.0 or 0.3 mM of malate is produced after 5 h of irradiation using a 500 W high-pressure Hg arc lamp, respectively.

Visible-light-driven malate production using chlorophyll derivative, zinc chlorin e6 (ZnCe6; chemical structure is shown in Fig. 43) as PS in the system shown in Fig. 52(a) has also been reported.[176]

After 3 h of irradiation using a 250 W tungsten lamp ($\lambda >$ 365 nm), 0.65 mM of malate production is observed using the system comprising NADH (3.0 mM), ZnCe6 (50 μM), MV^{2+} (1.0 mM), FNR (4.0 U), pyruvic acid (10 mM), sodium

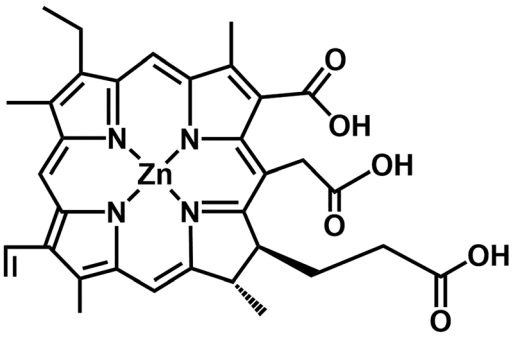

Fig. 43 Chemical structure of zinc chlorin e6 (ZnCe6).

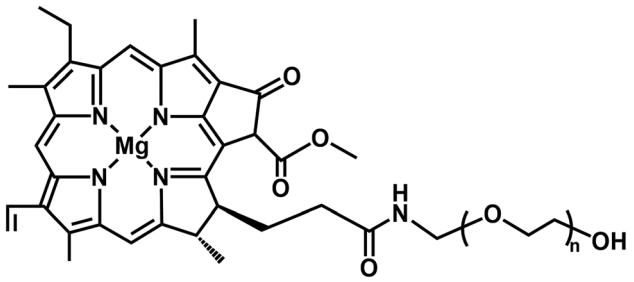

Fig. 44 Chemical structure of PEG-Chl-*a*.

bicarbonate (10 mM), $NADP^+$ (10 mM) and ME (4.5 U) in 50 mM of Bis–Tris buffer (3.0 mL; pH 8.0).

It has been reported that NADPH can be regenerated even in the absence of MV^{2+} using PEG-Chl-*a* (the chemical structure is shown in Fig. 44) as PS, as depicted in Fig. 42(a).[167]

Using PEG-Chl-*a* (15 μM) as a PS, malate production in the system comprising sodium ascorbate (6.0 mM), sodium bicarbonate (180 mM), magnesium chloride (15 mM), sodium pyruvate (0.8 mM), $NADP^+$ (3.2 mM), FNR (2.5 U) and ME (5.0 U) in 50 mM of phosphate buffer (10 mL; pH 7.4) during irradiation using a 60 W incandescent lamp from a distance of 10 cm (light intensity, 200 J m^{-2} s^{-1}) is observed, and 0.15 mM of malate is produced after 4 h irradiation.

In addition, the optical activity of the malate produced in the reaction system introduced in this section, D- or L-, has not been identified.

Next, a research example on visible-light-driven malate production with ME added as a catalyst, as depicted in Fig. 42(b), is introduced. Visible-light-driven L-malate production from sodium bicarbonate and pyruvate using the system comprising triethanol amine (TEOA) as ED, water-soluble zinc porphyrin, $ZnTPPS^{4-}$ as PS, $[RhCp^*(bpy)(H_2O)]^{2+}$, NAD^+, and ME is introduced.[177]

After 5 h of irradiation using a 250 W Halogen lamp ($\lambda >$ 390 nm), 0.16 mM of L-malate production is observed using the system comprising sodium pyruvate (5.0 mM), TEOA (0.2 M), $ZnTPPS^{4-}$ (10 μM), $[RhCp^*(bpy)(H_2O)]^{2+}$ (10 μM), NAD^+ (0.5 mM), sodium bicarbonate (100 mM), magnesium chloride (5.0 mM) and ME (0.7 U) in CO_2-saturated 500 mM HEPES–NaOH buffer (5.0 mL; pH 7.3). However, 40 μM of L-malate production is observed under Ar-saturated 500 mM HEPES–NaOH buffer (pH 7.3). This result suggests that the equilibrium between gaseous CO_2 in the gas phase and bicarbonate ions in the sample solution is important for ME-catalysed L-malate production. In particular, this sealed isochoric system has the problem of a decrease in pressure within the system because gaseous CO_2 in the gas phase of the reaction vessel is captured by the weak basic buffer solution. Therefore, visible-light-driven L-malate production has also been reported using an isobaric reaction system attached to a balloon filled with 1 L of CO_2 gas.[178] After 5 h of irradiation using a 250 W Halogen lamp ($\lambda >$ 390 nm), *ca.* 0.16 mM of L-malate production is observed using the system comprising sodium pyruvate (5.0 mM), TEOA (0.2 M), $ZnTPPS^{4-}$ (10 μM), $[RhCp^*(bpy)(H_2O)]^{2+}$ (10 μM), NAD^+ (0.5 mM), magnesium chloride (5.0 mM) and ME (0.7 U) in 500 mM HEPES–NaOH buffer (5.0 mL; pH 7.3). A balloon filled with 1 L of CO_2 gas is attached to the reaction vessel, and the pressure inside the reaction system is maintained at 1.0 atm. Furthermore, no sodium bicarbonate is added to the reaction sample. The increase in L-malate over the irradiation time indicates that bicarbonate is continuously captured from CO_2 gas and fixed to pyruvate by ME together with NADH regenerated by visible light irradiation. Using this isobaric system, L-malate can be produced directly using gaseous CO_2 as a raw material.

In addition, visible-light-driven L-malate production using a water-soluble cationic zinc porphyrin, zinc tetrakis(4-*N*,*N*,*N*-trimethylaminophenyl)porphyrin ($ZnTMAP^{4+}$; chemical structure is shown in Fig. 45), as a PS has also been reported.[179]

After 5 h of irradiation using a 250 W Halogen lamp ($\lambda >$ 390 nm), *ca.* 0.25 mM of L-malate production is observed with the system comprising sodium pyruvate (5.0 mM), TEOA (0.2 M), $ZnTMAP^{4+}$ (50 μM), $[RhCp^*(bpy)(H_2O)]^{2+}$ (10 μM), NAD^+ (0.5 mM), magnesium chloride (5.0 mM) and ME (0.7 U) in 500 mM HEPES–NaOH buffer (5.0 mL; pH 7.3). A balloon filled with 1 L of CO_2 gas is attached to the reaction vessel, and the pressure inside the reaction system is maintained at 1.0 atm. Using $ZnTMAP^{4+}$ as a photosensitiser, approximately 1.5 times more L-malate is produced than in the system with $ZnTPPS^{4-}$. As a stable NAD^+ reduction, NADH

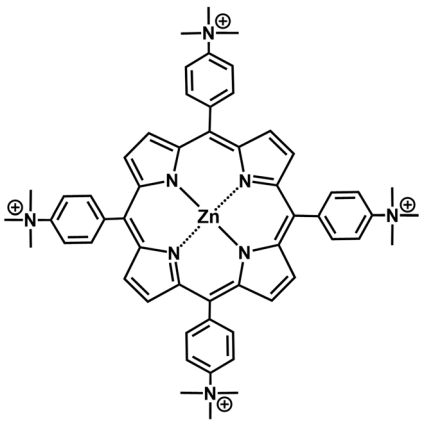

Fig. 45 Chemical structure of $ZnTMAP^{4+}$.

in a system comprising TEOA and $[Cp^*Rh(bpy)(H_2O)]^{2+}$ with $ZnTMAP^{4+}$ as a PS compared to a system using $ZnTPPS^{4-}$; thus, the efficiency of visible-light-driven L-malate production is improved using $ZnTMAP^{4+}$.

As described above, L-malate production from CO_2 and pyruvate using ME as a photoredox catalyst is achieved. However, in the production of L-malate using ME as a catalyst, L-lactate is produced through the reduction of pyruvate under a low concentration of CO_2 or bicarbonate. Therefore, a system mimicking the mitochondrial pyruvate malate shuttle,[180,181] consisting of pyruvate carboxylase (PC; EC 6.4.1.1) and malate dehydrogenase (MDH; EC 1.1.1.37) in the presence of ATP and NADH, is proposed to produce L-malate using low-concentration CO_2 as a feedstock.

Fig. 46 shows the PC-catalysed oxaloacetate production from pyruvate and bicarbonate in the presence of ATP (a) and MDH-catalysed L-malate production based on oxaloacetate reduction in the presence of NADH (b). Using a dual-enzyme consisting of PC and MDH, L-malate can be produced from pyruvate and bicarbonate *via* oxaloacetate as an intermediate. In addition, using PC as a catalyst, no reduction process of pyruvate is involved to suppress L-lactate production and enable the use of low-concentration CO_2 as a raw material.[182,183]

Visible-light-driven L-malate production from pyruvate and CO_2 using a system comprising TEOA, $ZnTMAP^{4+}$, $[RhCp^*(bpy)(H_2O)]^{2+}$, NAD^+, ATP, acetyl-CoA, PC and MDH has been reported.[184] Fig. 47 shows the time dependence of L-malate production using a system comprising sodium pyruvate (5.0 mM), acetyl-CoA (1.0 mM), magnesium chloride (5.0 mM), sodium ATP (5.0 mM), TEOA (0.2 M), $ZnTMAP^{4+}$ (50 μM), NAD^+ (5.0 mM), $[Rh\ Cp^*(bpy)(H_2O)]^{2+}$ (0.1 mM), PC (1.0 U) and MDH (20 U) in 5.0 mL of 500 mM HEPES–NaOH buffer solution (pH 7.8) under visible-light irradiation using a 250 W halogen lamp ($\lambda > 390$ nm). A balloon filled with 1 L of a gas mixture of N_2 and CO_2 is attached to the reaction vessel, and the pressure inside the reaction system is maintained at 1.0 atm. As shown in Fig. 47, more L-malate production is observed under 15.0% CO_2 conditions compared with under 100% CO_2 conditions. The change in the pH of the sample solution during the reaction is measured, and the pH decreases from 7.8 to 7.0 under 100% CO_2 conditions. However, no change is observed in the pH of the sample solution during reaction under 15.0% CO_2 conditions. It has been reported that the rate of visible-light-driven NADH regeneration decreases as the pH of the sample solution decreases. Therefore, the low L-malate production under 100% CO_2 conditions is due to a decrease in NADH regeneration induced by a drop in pH during irradiation. By complementing the catalytic function of ME with PC and MDH, visible-light-driven L-malate production using low-concentration CO_2 as a direct feedstock is accomplished.

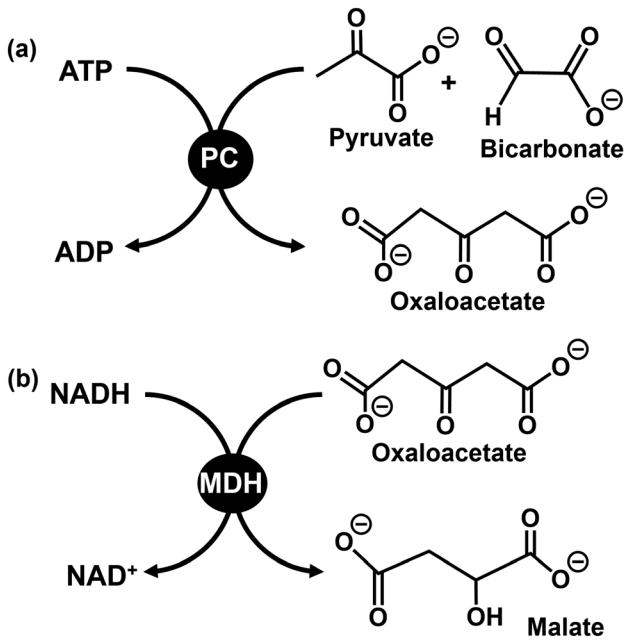

Fig. 46 PC-catalysed oxaloacetate production from pyruvate and bicarbonate in the presence of ATP (a). MDH-catalysed L-malate production based on the reduction of oxaloacetate in the presence of NADH (b).

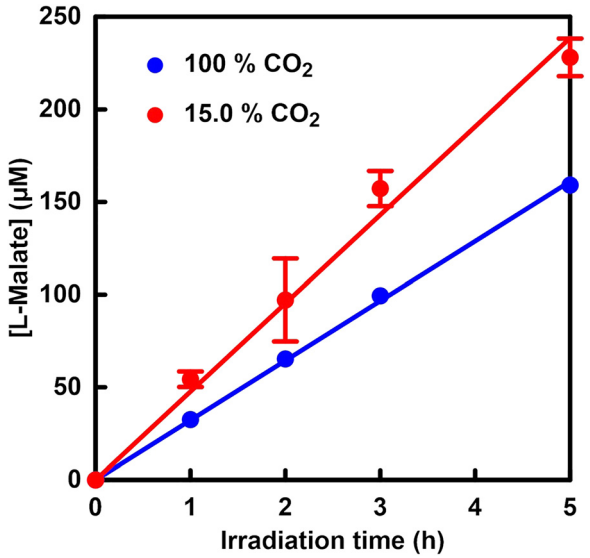

Fig. 47 Time-dependent concentration of L-malate in a system comprising sodium pyruvate, acetyl-CoA, magnesium chloride, sodium ATP, TEOA, $ZnTMAP^{4+}$, NAD^+, $[Rh\ Cp^*(bpy)(H_2O)]^{2}$, PC and MDH in an HEPES–NaOH buffer solution (pH 7.8) under visible-light irradiation. The gas phase of the reaction vessel was introduced with 15.0 (red) or 100% CO_2 (blue) gas. Reproduced with permission from ref. 184. Copyright 2025, the American Chemical Society.

Finally, an overview of the visible-light-driven L-malate production from CO_2 and pyruvate using a photocatalytic dye and enzyme hybrid system, as reviewed in this section, is summarized in Table 2.

Visible-light-driven fumarate production from CO_2 and pyruvate with the photocatalytic dye and enzyme hybrid system

Malate is a precursor to PMLA but can be converted by dehydration to fumarate, a precursor to a more versatile biodegradable plastic. In other words, by incorporating FUM in addition to ME, fumarate can be produced from CO_2.

Table 2 Summary of the visible-light-driven malate production from carbonate species and pyruvate using a photocatalytic dye and enzyme hybrid system

System	Malate production (mM)	Ref.
RSH (19 mM), $[Ru(bpy)_3]^{2+}$ (21 μM), MV^{2+} (0.19 mM), $NADP^+$(0.18 mM), pyruvic acid (47 mM), sodium bicarbonate (0.20 M), manganese chloride (95 μM), FNR (0.2 U) and ME (1.33 U)	1.5	156
RSH (27 mM), CdS or TiO_2/clay (1.25 mM), MV^{2+} (1.0 mM), $NADP^+$ (0.1 mM), pyruvic acid (2.0 mM), FNR (0.2 U) and ME (1.0 U) in a CO_2-saturated buffer	0.2 for CdS 0.06 for TiO_2/clay	175
NADH (3.0 mM), ZnCe6 (50 μM), MV^{2+} (1.0 mM), FNR (4.0 U), pyruvic acid (10 mM), sodium bicarbonate (10 mM), $NADP^+$ (10 mM) and ME (4.5 U)	0.21	162
Sodium ascorbate (6.0 mM), PEG-Chl-*a* (15 μM), sodium bicarbonate (180 mM), magnesium chloride (15 mM), sodium pyruvate (0.8 mM), $NADP^+$ (3.2 mM), FNR (2.5 U) and ME (5.0 U)	0.0375	167
Sodium pyruvate (5.0 mM), TEOA (0.2 M), $ZnTPPS^{4-}$ (10 μM), $[RhCp^*(bpy)(H_2O)]^{2+}$ (10 μM), NAD^+ (0.5 mM), sodium bicarbonate (100 mM), magnesium chloride (5.0 mM) and ME (0.7 U) in CO_2-saturated buffer	0.032	177
Sodium pyruvate (5.0 mM), TEOA (0.2 M), $ZnTPPS^{4-}$ (10 μM), $[RhCp^*(bpy)(H_2O)]^{2+}$ (10 μM), NAD^+ (0.5 mM), magnesium chloride (5.0 mM) and ME (0.7 U) in CO_2-saturated buffer	0.032	178
Sodium pyruvate (5.0 mM), TEOA (0.2 M), $ZnTMAP^{4+}$ (50 μM), $[RhCp^*(bpy)(H_2O)]^{2+}$ (10 μM), NAD^+ (0.5 mM), magnesium chloride (5.0 mM) and ME (0.7 U) in CO_2-saturated buffer	0.050	179
sodium pyruvate (5.0 mM), acetyl-CoA (1.0 mM), magnesium chloride (5.0 mM), sodium ATP (5.0 mM), TEOA (0.2 M), $ZnTMAP^{4+}$ (50 μM), NAD^+ (5.0 mM), $[RhCp^*(bpy)(H_2O)]^{2+}$ (0.1 mM), PC (1.0 U) and MDH (20 U)	0.23 (15% CO_2) 0.15 (100% CO_2)	184

The production of fumarate from CO_2 as a raw material by hybridising a visible-light-driven NADH regeneration system consisting of a photocatalytic dye and a catalyst with a dual enzyme consisting of ME and FUM is introduced in this section.

As mentioned above, visible-light-driven fumarate production from CO_2 and pyruvate is achieved using a system comprising RSH, $[Ru(bpy)_3]^{2+}$, MV^{2+}, $NADP^+$, FNR, ME and FUM. No other studies have been reported on the production of fumarate using visible-light-driven NADPH regeneration catalysed by FNR in the presence of ME and FUM.

First, visible-light-driven fumarate production from pyruvate and bicarbonate instead of CO_2 gas using a system comprising TEOA, $ZnTPPS^{4-}$, $[RhCp^*(bpy)(H_2O)]^{2+}$, NAD^+, ME and FUM is introduced.[172] The sample solution consists of TEOA (0.2 M), $ZnTPPS^{4-}$ (10 μM), $[RhCp^*(bpy)(H_2O)]^{2+}$ (10 μM), NAD^+ (0.5 mM), sodium pyruvate (5.0 mM), sodium bicarbonate (100 mM), magnesium chloride (5.0 mM), ME (0.7 U) and FUM (0.5 U) in 5.0 mL of CO_2-saturated 500 mM HEPES–NaOH buffer (5.0 mL; pH 7.8). The sample solution is irradiated with visible light using a 250 W halogen lamp ($\lambda > 390$ nm). Using this system, the concentrations of L-malate and fumarate are estimated to be 194 and 48 μM, respectively, after 5 h of irradiation. Although the production of L-malate tends to reach a constant concentration, the fumarate concentration linearly increases during irradiation. Visible-light-driven fumarate production has also been reported using an isobaric reaction system attached to a balloon filled with 1 L of CO_2 gas.[178] After 5 h of irradiation using a 250 W halogen lamp ($\lambda > 390$ nm), *ca.* 190 and 49 μM of L-malate and fumarate production are observed using a system comprising sodium pyruvate (5.0 mM), TEOA (0.2 M), $ZnTPPS^{4-}$ (10 μM), $[RhCp^*(bpy)(H_2O)]^{2+}$ (10 μM), NAD^+ (0.5 mM), magnesium chloride (5.0 mM), ME (0.7 U) and FUM (0.5 U) in 500 mM HEPES–NaOH buffer (5.0 mL; pH 7.8). A balloon filled with 1 L of CO_2 gas is attached to the reaction vessel, and the pressure inside the reaction system is maintained at 1.0 atm. Furthermore, no sodium bicarbonate is added to the reaction sample. No significant difference in fumarate production is observed under 100% CO_2 conditions in the gas phase and the presence of bicarbonate conditions. However, it has been reported that as the CO_2 ratio in the mixed gas in the balloon decreases, the production of L-malate and fumarate also decreases.

Using a system comprising TEOA, $ZnTPPS^{4-}$, $[RhCp^*(bpy)(H_2O)]^{2+}$, NAD^+, ME and FUM, the concentration of fumarate produced remains significantly lower than that of L-malate, whether CO_2 gas or bicarbonate is used as the feedstock. For example, it has been reported that the addition of phosphate improves the catalytic activity of FUM for the production of fumarate based on the dehydration of L-malate.[185] In other words, anionic or cationic substances may control the catalytic activity of FUM. Thus, the effect of water-soluble zinc porphyrin on the FUM-catalysed dehydration of L-malate to produce fumarate has been investigated. The effects of water-soluble zinc porphyrins, $ZnTPPS^{4-}$ and $ZnTMAP^{4+}$, as well as zinc tetra(4-carboxyphenyl)porphyrin ($ZnTCPP^{4-}$) and zinc tetrakis-(4-methylpyridyl)porphyrin ($ZnTMPyP^{4+}$) on the enzyme activity of FUM for fumarate production have been investigated. Fig. 48 shows the chemical structures of $ZnTCPP^{4-}$ and $ZnTMPyP^{4+}$.

As shown in Fig. 49, the addition of cationic zinc porphyrins, $ZnTMPyP^{4+}$ or $ZnTMAP^{4+}$, did not alter fumarate production from L-malate by FUM compared to the control experiment. By adding anionic zinc porphyrins, $ZnTCPP^{4-}$ or $ZnTPPS^{4-}$, in contrast, fumarate production from L-malate with FUM is

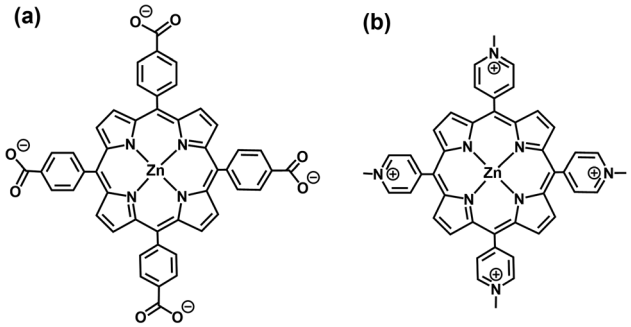

Fig. 48 Chemical structures of $ZnTCPP^{4-}$ (a) and $ZnTMPyP^{4+}$ (b).

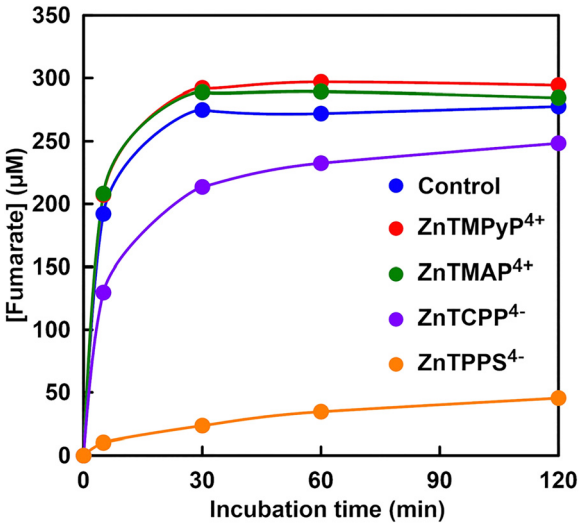

Fig. 49 Time-dependent fumarate production from L-malate with FUM in the presence of zinc porphyrin during incubation. Reproduced with permission from ref. 186. Copyright 2023, The Royal Society of Chemistry.

suppressed. In particular, fumarate production with FUM is strongly inhibited in the presence of $ZnTPPS^{4-}$.

It is suggested that the sulfo-group bonded to zinc porphyrin has a stronger effect on the catalytic activity of FUM than that of the carboxy-group.[186]

Here, we focus on the structural interactions between FUM and water-soluble zinc porphyrins. As presented in this section, FUM is an enzyme derived from porcine heart. The three-dimensional structures of porcine heart-derived and related FUMs have been reported.[187–189] It has been reported that porcine heart-derived FUM is composed of four subunits. FUM has four active sites (site A) with high affinity for substrates, as well as an additional binding site (site B) with low affinity for substrates.[189] Fig. 50 is a schematic diagram showing the active high-affinity substrate binding sites (A) and low-affinity binding sites (B) in the FUM.

For example, tetracarboxylic acid, benzene-1,2,4,5-tetracarboxylate and sulfate have been reported as strong inhibitors for FUM.[189] In particular, it is found that one molecule of benzene-1,2,4,5-tetracarboxylic acid can bind to both sites A and B simultaneously, and that four carboxyl groups of

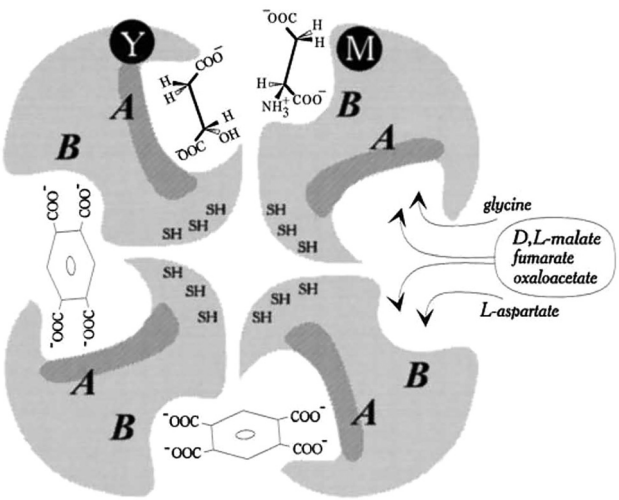

Fig. 50 Schematic showing the active high-affinity substrate binding sites (A) and low-affinity binding sites (B) in FUM. Reproduced with permission from ref. 189. Copyright 1998 ASBMB. Currently published by Elsevier Inc.; originally published by the American Society for Biochemistry and Molecular Biology. Creative Commons CC-BY-NC license.

benzene-1,2,4,5-tetracarboxylic acid per FUM molecule bind with high affinity, acting as bridges between the two subunits. These results suggest that the four benzenesulfonate groups of $ZnTPPS^{4-}$ also bind with high affinity to the substrate-binding sites (sites A and B) of FUM, inhibiting the dehydration of L-malate and reducing the production of fumarate.

Therefore, a visible-light-driven fumarate production system has been reported that uses $ZnTMAP^{4+}$ as PS instead of $ZnTPPS^{4-}$, which does not affect FUM enzyme activity.[179] Visible-light-driven fumarate production has also been reported using an isobaric reaction system attached to a balloon filled with 1 L of CO_2 gas.[179,190] After 5 h of irradiation using a 250 W halogen lamp ($\lambda > 390$ nm), *ca.* 97 μM of fumarate production is observed using a system comprising sodium pyruvate (5.0 mM), TEOA (0.2 M), $ZnTMAP^{4+}$ (50 μM), $[RhCp^*(bpy)(H_2O)]^{2+}$ (10 μM), NAD^+ (0.5 mM), magnesium chloride (5.0 mM), ME (0.7 U) and FUM (0.5 U) in 500 mM HEPES–NaOH buffer (5.0 mL; pH 7.8). A balloon filled with 1 L of CO_2 gas is attached to the reaction vessel, and the pressure inside the reaction system is maintained at 1.0 atm. Fig. 51 shows the fumarate concentration using $ZnTMAP^{4+}$ or $ZnTPPS^{4-}$ after 5 h of irradiation.

The efficiency of visible-light-driven fumarate production from pyruvate and gaseous CO_2 using $ZnTMAP^{4+}$ as the PS in a system combining NAD^+ reduction with $[RhCp^*(bpy)(H_2O)]^{2+}$ and a dual-biocatalyst consisting of ME and FUM in the presence of TEOA is improved by approximately 2.0 times that produced in the system using $ZnTPPS^{4-}$, a conventional PS.

As a relevant study of this system, fumarate production from pyruvate and bicarbonate using a core–shell type of benzodiimidazole oligomer-$BaSO_4$-immobilised $[RhCp^*(bpy)(H_2O)]^{2+}$ (BaPP@BDO-Rh) instead of water-soluble zinc porphyrin as a visible-light sensitising material with dual-biocatalyst consisting of ME and FUM has been reported, as shown in Fig. 52(A).[191] In this study, ME and FUM are expressed in *E. coli* strain DE3

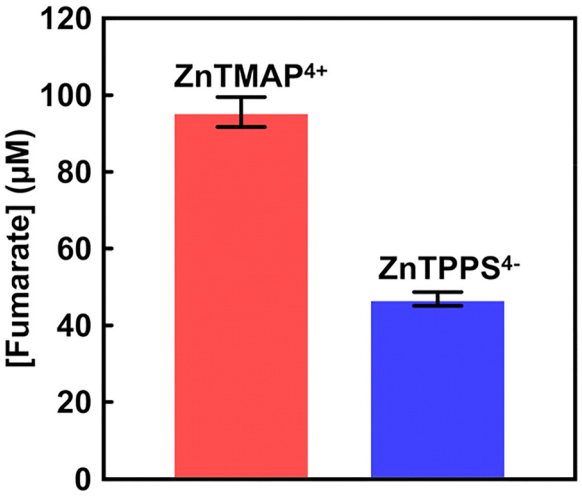

Fig. 51 Concentration of fumarate production in a system comprising sodium pyruvate, magnesium chloride, TEOA, $[RhCp^*(bpy)(H_2O)]^{2+}$, NAD^+, ME, FUM and CO_2 gas in the presence of $ZnTMAP^{4+}$ (red) or $ZnTPPS^{4-}$ (blue) after 5 h of irradiation. Reproduced with permission from ref. 179. Copyright 2023, The Royal Society of Chemistry.

using the pET28a vector; then, the enzymes are purified for use in this reaction. The ME and FUM are designated MaeB and FumC, respectively. The sample solution consists of TEOA (1.0 M), 1 g L^{-1} BaPP@BDO-Rh, NAD^+ (1.0 mM), sodium pyruvate (5.0 mM), sodium bicarbonate (100 mM), magnesium chloride (5.0 mM), MaeB (1.0 U) and FumC (1.0 U) in 3.0 mL of 100mM phosphate buffer. The sample solution is irradiated using a 100 W xenon lamp at room temperature as a visible light source. Using this system, the concentrations of L-malate and fumarate are estimated to be 114 and 63 μM, respectively, after 1 h of irradiation, as shown in Fig. 52(B).

In this study, ME and FUM are expressed in *E. coli strain DE*3 using the pET28a vector; then, the enzymes are purified for use in this reaction. The ME and FUM are designated MaeB and FumC, respectively. The sample solution consists of TEOA (1.0 M), 1 g L^{-1} BaPP@BDO-Rh, NAD^+ (1.0 mM), sodium pyruvate (5.0 mM), sodium bicarbonate (100 mM), magnesium chloride (5.0 mM), MaeB (1.0 U) and FumC (1.0 U) in 3.0 mL of 100 mM phosphate buffer. The sample solution is irradiated using a 100 W xenon lamp at room temperature as a visible light source. Using this system, the concentrations of L-malate and fumarate are estimated to be 114 and 63 μM, respectively, after 1 h of irradiation, as shown in Fig. 52(B).

However, no L-malate and fumarate production are observed under dark conditions. It is believed that malate production under irradiation and dark conditions in this reference is reversed. Moreover, 79 μM of fumarate is produced using this system after 3 h of irradiation. The production of L-malate and fumarate tends to reach a constant concentration during irradiation in this system.

Visible-light-driven fumarate production from pyruvate and CO_2 using a system comprising TEOA, $ZnTMAP^{4+}$, $[RhCp^*(bpy)(H_2O)]^{2+}$, NAD^+, ATP, acetyl-CoA, PC, MDH and FUM has been reported.[184] L-Malate and fumarate production are observed

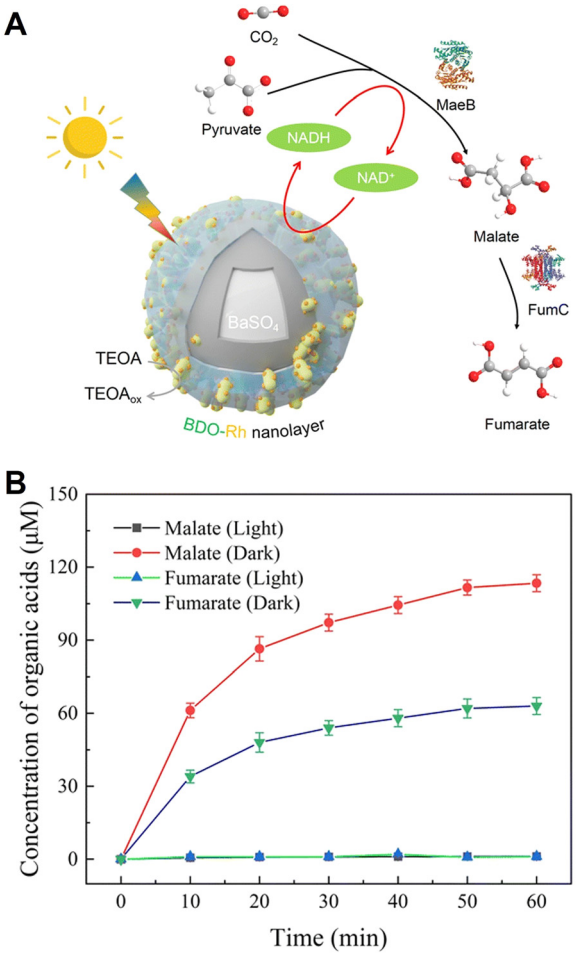

Fig. 52 Schematic of the visible-light-driven fumarate production from pyruvate and CO_2 using a system comprising TEOA, BaPP@BDO-Rh, NAD^+, MaeB and FumC (A). Time-dependent malate and fumarate production from pyruvate and CO_2 using the system comprising TEOA, BaPP@BDO-Rh, NAD^+, MaeB and FumC (B). Reproduced with permission from ref. 191. Copyright 2023, The Royal Society of Chemistry.

using a system comprising sodium pyruvate (5.0 mM), acetyl-CoA (1.0 mM), magnesium chloride (5.0 mM), sodium ATP (5.0 mM), TEOA (0.2 M), $ZnTMAP^{4+}$ (50 μM), NAD^+ (5.0 mM), $[RhCp^*(bpy)(H_2O)]^{2+}$ (0.1 mM), PC (1.0 U), MDH (20 U) and FUM (0.5 U) in 5.0 mL of 500 mM HEPES–NaOH buffer solution (pH 7.8) under visible-light irradiation with a 250 W halogen lamp ($\lambda > 390$ nm). A balloon filled with 1 L of a gas mixture of N_2 and CO_2 is attached to the reaction vessel, and the pressure inside the reaction system is maintained at 1.0 atm. Under conditions using a gas mixture containing 15% CO_2, *ca.* 213 and 57.6 μM of L-malate and fumarate are produced after 5 h of irradiation, respectively. Furthermore, no significant difference is observed between L-malate and fumarate production under mixed gas conditions containing 50% CO_2.

However, it has also been shown that L-malate and fumarate production is reduced by approximately half under mixed gas conditions containing 100% CO_2 or 2% CO_2. By complementing the catalytic function of ME with PC and MDH and using it

Table 3 Summary of the visible-light-driven fumarate production from carbonate species and pyruvate using a photocatalytic dye and enzyme hybrid system

System	Fumarate production (μM)	Ref.
TEOA (0.2 M), $ZnTPPS^{4-}$ (10 μM), $[RhCp^*(bpy)(H_2O)]^{2+}$ (10 μM), NAD^+ (0.5 mM), sodium pyruvate (5.0 mM), sodium bicarbonate (100 mM), magnesium chloride (5.0 mM), ME (0.7 U) and FUM (0.5 U)	48 (5 h)	177
sodium pyruvate (5.0 mM), TEOA (0.2 M), $ZnTPPS^{4-}$ (10 μM), $[RhCp^*(bpy)(H_2O)]^{2+}$ (10 μM), NAD^+ (0.5 mM), magnesium chloride (5.0 mM), ME (0.7 U) and FUM (0.5 U) in a CO_2-saturated buffer	49 (5 h)	178
sodium pyruvate (5.0 mM), TEOA (0.2 M), $ZnTMAP^{4+}$ (50 μM), $[RhCp^*(bpy)(H_2O)]^{2+}$ (10 μM), NAD^+ (0.5 mM), magnesium chloride (5.0 mM), ME (0.7 U) and FUM (0.5 U) in a CO_2-saturated buffer	97 (5 h)	179
TEOA (1.0 M), 1 g L^{-1} BaPP@BDO-Rh, NAD^+ (1.0 mM), sodium pyruvate (5.0 mM), sodium bicarbonate (100 mM), magnesium chloride (5.0 mM), MaeB (1.0 U) and FumC (1.0 U)	63 (1 h)	191
sodium pyruvate (5.0 mM), acetyl-CoA (1.0 mM), magnesium chloride (5.0 mM), sodium ATP (5.0 mM), TEOA (0.2 M), $ZnTMAP^{4+}$ (50 μM), NAD^+ (5.0 mM), $[RhCp^*(bpy)(H_2O)]^{2+}$ (0.1 mM), PC (1.0 U), MDH (20 U) and FUM (0.5 U) in a 15% CO_2-saturated buffer	58 (5 h)	184

together with FUM, visible-light-driven fumarate production can be achieved using low-concentration CO_2 (approximately 15%) as a direct feedstock.

Finally, an overview of the visible-light-driven fumarate production from CO_2 and pyruvate using a photocatalytic dye and enzyme hybrid system, as reviewed in this section, is summarized in Table 3.

Major challenges and future trends

Here, the problems and prospects for future demonstrations of the systems introduced in this study will be discussed. First, we discuss the challenges to the practical application of visible-light-driven plastic precursor production from CO_2 using a photocatalyst and microbial cell hybrid system. The reaction scale of visible-light-driven plastic precursor production from CO_2 using a photocatalyst and microbial cell hybrid system will be discussed. As described in the paper, the reaction scale of the hybrid system is approximately 1.0 L at the maximum laboratory level. Scaling up this system for material production involves several significant challenges, including maintaining product quality stability, ensuring process efficiency, and, in some cases, complying with regulatory requirements.

In addition, although Xe and halogen lamps are currently used as visible light sources, it will be necessary to directly utilize solar-light in the future, and the design of the reaction vessel for this purpose will be an important factor. Visible-light-driven plastic precursor production from CO_2 using a photocatalyst and microbial cell hybrid system is still under development, and future developments in chemical engineering will likely pave the way for its practical application through the design of the reaction apparatus. However, a hybrid system has the advantage of efficiently promoting CO_2 conversion within microbial cells through induced electrons from solar energy efficiently absorbed using semiconductor photocatalysts and organic dyes. This suggests the potential for more efficient utilization of solar energy compared to CO_2 conversion by photosynthetic microorganisms such as microalgae. In other words, it would be possible to apply a CO_2 conversion apparatus that utilizes the photosynthetic function of microalgae and other organisms, which is already in practical use, to a hybrid system.

Visible-light-driven plastic precursor production from CO_2 using a photocatalyst and microbial cell hybrid system is attracting attention as an innovative technology that can achieve both the resolution of global challenges and economic growth, but currently, high costs are a major challenge. In particular, this system relies on the growth of microorganisms, resulting in low productivity and increased equipment and purification costs. To overcome these challenges, it is necessary to work on improving large-scale culture technology, advanced separation and purification technology, and the development of bioreactors. Furthermore, the production of high-value-added biodegradable plastics and their precursors from CO_2 will further enhance the value of this system.

Next, we focus on the direct use of CO_2 gas in hybrid systems. In the visible-light-driven plastic precursor production from CO_2 using a photocatalyst and microbial cell hybrid system, a mixed gas with an approximate N_2 to CO_2 ratio of 80 : 20 is used as the raw material. This is a mixed gas composition optimized for substance production in microbial cells. In some cases, adding hydrogen to a gas mixture can improve the efficiency of producing the desired substance. In particular, in the case of visible-light-driven plastic precursor production from CO_2 using a photocatalyst and microbial cell hybrid system, the use of mixed gases, such as exhaust gases emitted from coal-fired power plants, has not yet been considered.

In a visible-light-driven biodegradable plastic precursor production system using photocatalytic dyes and multi-enzymes, however, it is possible to change the composition of the CO_2 gas used as a raw material. In other words, this system has the

potential to use CO_2 diluted with N_2, *etc.*, emitted from coal-fired power plants, as a raw material. It has been reported that exhaust gases contain approximately 0.02–0.3% NO_x and SO_2.[192] Here, a significant advantage of the visible-light-driven biodegradable plastic precursor production system using photocatalytic dyes and multi-enzymes is that it allows for the capture of CO_2 gas in the reaction solution using a weakly basic buffer. In addition, because a buffer solution is used, even if NO_x or SO_2 is captured, the pH of the reaction solution does not change, and it is expected that this does not significantly affect the total process.

Finally, we discuss the hybrid systems introduced in this study from the perspective of life cycle analysis (LCA). There are currently no reported cases of LCA estimation for photocatalysts, biocatalysts, or microbial cell hybrid systems. Therefore, this approach depending on reports on life cycle assessments (LCAs) for hydrogen production based on water splitting using semiconductor photocatalysts is discussed.[193] According to this report, in the production of 1 kg of hydrogen using semiconductor photocatalysts, greenhouse gases are mainly released during the preparation of the photocatalyst (95.87%). However, we discuss LCA for biocatalytic CO_2 conversion based on bioelectrochemical methods using microbial cells.[194] LCA evaluations of this system indicate that its carbon footprint is comparable to that of fermentation or plant-based manufacturing methods. In other words, it goes without saying that a hybrid system comprising semiconductor photocatalysts and microbial cells also has the potential to contribute to CO_2 reduction. These conclusions suggest that at this stage, there are many hurdles to overcome before hybrid systems can achieve significant CO_2 reduction. However, the fact that value-added substances can be produced from CO_2 and biomass-derived compounds using light energy as a driving force suggests that it would be better to shift the focus from CO_2 reduction to its effective use as a raw material.

Conclusion and outlook

In this review article, focusing on biodegradable plastics and their precursor production from gaseous CO_2 using systems comprising visible-light-driven redox reactions with biocatalytic processes, the following types are outlined.

(1) The visible-light-driven production of biodegradable plastic precursors such as acetate, shikimic acid and acetoin from CO_2 using a hybrid system comprising the inorganic- or organic-based semiconductor photocatalyst and a microbial cell.

(2) The visible-light-driven production of biodegradable plastic PHB from CO_2 using a hybrid system comprising inorganic- or organic-based semiconductor photocatalysts and a microbial cell.

(3) The visible-light-driven production of biodegradable plastic precursor 3-hydroxybutyrate from acetone and CO_2 using a combination of NAD^+ reduction system of triethanolamine, water-soluble zinc porphyrin, $[Cp^*Rh(bpy)(H_2O)]^{2+}$ and a cell extract including dual-enzymes.

(4) The visible-light-driven production of biodegradable plastic precursors L-malate fumarate from bio-based pyruvate and CO_2 using a photoredox system consisting of an electron donor, a photosensitizer, an electron mediator and an enzyme-based biocatalyst.

In the future, it is expected that innovative technologies with a photo/biocatalytic hybrid system will be developed for the effective and practical use of the visible-light-driven production of biodegradable plastics and their precursors from gaseous CO_2 and small organic molecules. Therefore, the research introduced in this article contributes to the CO_2 fixation, and to alternative plastic or its precursor production for a sustainable society. These systems can fix gaseous CO_2 in small organic molecules and convert it into high-value-added materials, resulting in the long-term storage of CO_2 in molecules.

Conflicts of interest

There are no conflicts to declare.

Data availability

No primary research results have been included, and no new data were generated or analysed as part of this review article.

Acknowledgements

Our work introduced in this review is partially supported by Grant-in-Aid for Specially Promoted Research (23H05404), Scientific Research (B) (25K01584), (23K23140), (22H01872), and (22H01871).

Notes and references

1 G. Q. Chen and M. K. Patel, *Chem. Rev.*, 2012, **112**, 2082.
2 R. Kajaste and P. Oinas, *AIMS Environ. Sci.*, 2021, **8**, 371.
3 J. Hammer, M. H. Kraak and J. R. Parsons, *Rev. Environ. Contam. Toxicol.*, 2012, **220**, 1.
4 T. R. Walker and D. Xanthos, *Resour., Conserv. Recycl.*, 2018, **133**, 99.
5 P. Stoett, V. M. Scrich, C. I. Elliff, M. M. Andrade, N. de, M. Grilli and A. Turra, *World Dev.*, 2024, **184**, 106756.
6 R. Ciriminna and M. Pagliaro, *ChemistryOpen*, 2020, **9**, 8.
7 *Handbook of Bioplastics and Biocomposites Engineering Applications*, ed S. Pilla, Wiley-Scrivener, Salem (MA), 2011.
8 P. Skoczinski, M. Carus, G. Tweddle, P. Ruiz, N. Hark, A. Zhang, D. de Guzman, J. Ravenstijn, H. Käb and A. Raschka, Bio-based Building Blocks and Polymers – Global Capacities, *Production and Trends*, 2023–2028, GmbH, Hürth, Germany, 2024, 03.
9 C. Gioia, G. Giacobazzi, M. Vannini, G. Totaro, L. Sisti, M. Colonna, P. Marchese and A. Celli, *ChemSusChem*, 2021, **14**, 4167.
10 L. Filiciotto and G. Rothenberg, *ChemSusChem*, 2021, **14**, 56.
11 T. P. Haider, C. Völker, J. Kramm, K. Landfester and F. R. Wurm, *Angew. Chem., Int. Ed.*, 2019, **58**, 50.
12 S. Agarwal, *Macromol. Chem. Phys.*, 2020, **221**, 2000017.
13 A. Ammala, *Prog. Polym. Sci.*, 2011, **36**, 1015.
14 A. S. Al Hosni, J. K. Pittman and G. D. Robso, *Waste Manage.*, 2019, **97**, 105.
15 T. K. Chua, M. Tseng and M. K. Yang, *AMB Express*, 2013, **3**, 8.
16 L. Cosgrove, P. L. McGeechan, G. D. Robson and P. S. Handley, *Appl. Environ. Microbiol.*, 2007, **73**, 5817.
17 M. Karamanlioglu, A. Houlden and G. D. Robson, *Int. Biodeter. Biodegr.*, 2014, **95**, 301.

18 V. Nagarajan, A. K. Mohanty and M. Misra, *ACS Sustainable Chem. Eng.*, 2016, **4**, 2899.
19 O. Martin and L. Avérous, *Polymer*, 2001, **42**, 6209.
20 H. R. Kricheldorf and J. M. Jonté, *Polym. Bull.*, 1983, **9**, 276.
21 Y. K. Jung, T. Y. Kim and T. Yong, *Biotechnol. Bioeng.*, 2009, **105**, 161.
22 S. Bengtsson, A. Werker, M. Christensson and T. Welander, *Bioresour. Technol.*, 2008, **99**, 509.
23 S. Mohapatra, B. Sarkar, D. P. Samantaray, A. Daware, S. Maity, S. Pattnaik and S. Bhattacharjee, *Environ. Technol.*, 2017, **38**, 1.
24 S. Bengtsson, A. Werker and T. Welander, *Water Sci. Technol.*, 2008, **58**, 323.
25 F. Morgan-Sagastume, A. Karlsson, P. Johansson, S. Pratt, N. Boon, P. Lant and A. Werker, *Water Res.*, 2010, **44**, 5196.
26 F. Morgan-Sagastume, M. Hjort, D. Cirne, F. Gérardin, S. Lacroix, G. Gaval, L. Karabegovic, T. Alexandersson, P. Johansson, A. Karlsson, S. Bengtsson, M. V. Arcos-Hernández, P. Magnusson and A. Werker, *Bioresour. Technol.*, 2015, **181**, 78.
27 P. Chakravarty, V. Mhaisalkar and T. Chakrabarti, *Bioresour. Technol.*, 2010, **101**, 2896.
28 G. Q. Chen, *Chem. Soc. Rev.*, 2009, **38**, 2434.
29 K. Sudesh, H. Abe and Y. Doi, *Prog. Polym. Sci.*, 2000, **25**, 1503.
30 S. Chanprateep, *J. Biosci. Bioeng.*, 2010, **110**, 621.
31 R. Rai, T. Keshavarz, J. A. Roether, A. R. Boccaccini and I. Roy, *Mater. Sci. Eng. R*, 2011, **72**, 29.
32 P. K. Samantaray, A. Little, D. M. Haddleton, T. McNally, B. Tan, Z. Sun, W. Huang, Y. Ji and C. Wan, *Green Chem.*, 2020, **22**, 4055.
33 S. Mohapatra, S. Maity, H. R. Dash, S. Das, S. Pattnaik, C. C. Rath and D. Samantaray, *Biochem. Biophys. Rep.*, 2017, **12**, 206.
34 K. Yamane, H. Sato, Y. Ichikawa, K. Sunagawa and Y. Shigaki, *Polym. J.*, 2014, **46**, 76.
35 E. Göktürk, A. G. Pemba and S. A. Miller, *Polym. Chem.*, 2015, **6**, 3918.
36 M. Labet and W. Thielemans, *Chem. Soc. Rev.*, 2009, **38**, 3484.
37 J. O. Iroh, *Polymer Data Handbook*, ed J. E. Mark, Oxford University Press, New York, 1999, pp. 361–362.
38 H. Bittiger, R. H. Marchessault and W. D. Niegisch, *Acta Crystallogr., Sect. B: Struct. Crystallogr. Cryst. Chem.*, 1970, **26**, 1923.
39 R. A. Gross and B. Kalra, *Science*, 2002, **297**, 803.
40 Y. Ikada and H. Tsuji, *Macromol. Rapid Commun.*, 2000, **21**, 117.
41 T. F. Nelson, R. Baumgartner, M. Jaggi, S. M. Bernasconi, G. Battagliarin, C. Sinkel, A. Künkel, H. P. E. Kohler, K. McNeill1 and M. Sander, *Nat. Commun.*, 2022, **13**, 5691.
42 K. S. Savitha, B. R. Paghadar, M. S. Kumar and R. L. Jagadish, *Polym. Chem.*, 2022, **13**, 3562.
43 Y. Doi, K. Kasuya, H. Abe, N. Koyama, I. Shin-ichi, T. Koichi and Y. Yoshida, *Polym. Degrad. Stab.*, 1996, **51**, 281.
44 K. Kasuya, K. Takagi, S. Ishiwatari, Y. Yoshida and Y. Doi, *Polym. Degrad. Stab.*, 1998, **59**, 327.
45 A. Kilic, E. Yasar, H. İ. Önal, F. Koyuncu, M. Aydemir and F. Durap, *Energy Fuels*, 2025, **39**, 23241.
46 F. Tufano, C. Napolitano, M. Mazzeo, F. Grisi and M. Lamberti, *Biomacromolecules*, 2024, **25**, 4523.
47 S. Ye, S. Wang, L. Lin, M. Xiao and Y. Meng, *Adv. Ind. Eng. Polym. Res.*, 2019, **2**, 143.
48 Y. Y. Wang, J. W. Fan and D. J. Darensbourg, *Angew. Chem., Int. Ed.*, 2015, **54**, 10206.
49 D. Zhang, W. Wang, Z. Wang, D. Song, S. Liu, Y. Chen, X. Ma and L. Xia, *J. CO2 Util.*, 2025, **102**, 103236.
50 A. Stirbet, D. Lazár, Y. Guo and G. Govindjee, *Ann. Bot.*, 2019, **126**, 511.
51 A. N. Tikhonov and W. K. Subczynski, *Cell Biochem. Biophys.*, 2018, **77**, 47.
52 K. Asada, *Annu. Rev. Plant Physiol. Plant Mol. Biol.*, 1999, **50**, 601.
53 T. Shikanai, *Annu. Rev. Plant Biol.*, 2007, **58**, 199.
54 Y. Okegawa, Y. Kagawa, Y. Kobayashi and T. Shikanai, *Plant Cell Physiol.*, 2008, **49**, 825.
55 B. V. Trubitsin, A. V. Vershubskii, A. I. Priklonskii and A. N. Tikhonov, *J. Photochem. Photobiol., B*, 2015, **152**, 400.
56 J. Bassham, A. Benson and M. Calvin, *J. Biol. Chem.*, 1950, **185**, 781.
57 J. K. Sainis, D. N. Dani and G. K. Dey, *J. Plant Physiol.*, 2003, **160**, 23.
58 R. Hidese, M. Matsuda, T. Osanai, T. Hasunuma and A. Kondo, *ACS Synth. Biol.*, 2020, **9**, 260.
59 S. Ito, N. Koyama and T. Osanai, *Sci. Rep.*, 2019, **9**, 6038.
60 K. Maeda and K. Domen, *J. Phys. Chem. Lett.*, 2010, **1**, 2655.
61 S. J. A. Moniz, S. A. Shevlin, D. J. Martin, Z. X. Guoand and J. Tang, *Energy Environ. Sci.*, 2015, **8**, 731.
62 K. Takanabe, *ACS Catal.*, 2017, **7**, 8006.
63 Y. Wang, H. Suzuki, J. Xie, O. Tomita, D. J. Martin, M. Higashi, D. Kong, R. Abe and J. Tang, *Chem. Rev.*, 2018, **118**, 5201.
64 Q. Wang and K. Domen, *Chem. Rev.*, 2020, **120**, 919.
65 K. Kaiya, Y. Ueki, H. Kawamoto, K. Watanabe, S. Yoshino, Y. Yamaguchi and A. Kudo, *Chem. Sci.*, 2024, **15**, 16025.
66 R. N. Ivanovsky, Y. I. Fal, I. A. Berg, N. V. Ugolkova, E. N. Krasilnikova, O. I. Keppen, L. M. Zakharchuc and A. M. Zyakun, *Microbiology*, 1999, **145**, 1743.
67 H. G. Wood, *FASEB J.*, 1990, **5**, 156.
68 M. C. Evans, B. B. Buchanan and D. I. Arnon, *Proc. Natl. Acad. Sci. U. S. A.*, 1966, **55**, 928.
69 H. Berberoğlu, N. Barra, L. Pilon and J. Jay, *J. Appl. Microbiol.*, 2007, **104**, 105.
70 W. Eisenreich, G. Strauss, U. Werz, G. Fuchs and A. Bacher, *Eur. J. Biochem.*, 1993, **215**, 619.
71 S. W. Ragsdale, J. E. Clark, L. G. Ljungdahl and H. L. Drake, *J. Biol. Chem.*, 1983, **258**, 2364.
72 S. W. Ragsdale and E. Pierce, *Biochim. Biophys. Acta*, 2008, **1784**, 1873.
73 H. H. Cheng, J. C. Syu, S. Y. Tien and L. M. Whang, *Bioresour. Technol.*, 2018, **226**, 229.
74 Y. Xiea, S. Erşanb, X. Guana, J. Wanga, J. Shac, S. Xua, J. A. Wohlschlegelc, J. O. Park and C. Liu, *Proc. Natl. Acad. Sci. U. S. A.*, 2023, **120**, e2308373120.
75 M. Hermann, A. Teleki, S. Weitz, A. Niess, A. Freund, F. R. Bengelsdorf and R. Takors, *Microb. Biotechnol.*, 2020, **13**, 1831.
76 K. K. Sakimoto, A. B. Wong and P. Yang, *Science*, 2016, **351**, 74.
77 D. P. Cunningham and L. L. Lundie Jr., *Appl. Environ. Microbiol.*, 1993, **59**, 7.
78 H. Zhang, H. Liu, Z. Tian, D. Lu, Y. Yu, S. Cestellos-Blanco, K. K. Sakimoto and P. Yang, *Nat. Nanotechnol.*, 2018, **13**, 900.
79 K. K. Sakimoto, S. J. Zhang and P. Yang, *Nano Lett.*, 2016, **16**, 5883.
80 P. Gai, W. Yu, H. Zhao, R. Qi, F. Li, L. Liu, F. Lv and S. Wang, *Angew. Chem., Int. Ed.*, 2020, **59**, 7224.
81 B. Möller, R. Oßmer, B. H. Howard, G. Gottschalk and H. Hippe, *Arch. Microbiol.*, 1984, **139**, 388.
82 K. Nevin, T. L. Woodard, A. E. Franks, Z. M. Summers and D. R. Lovley, *mBio*, 2010, **1**, e00103.
83 D. R. Lovley and K. P. Nevin, *Curr. Opin. Biotechnol*, 2013, **24**, 385.
84 Y. He, S. Wang, X. Han, J. Shen, Y. Lu, J. Zhao, C. Shen and L. Qiao, *ACS Appl. Mater. Interfaces*, 2022, **14**, 23364.
85 Q. Wang, S. Kalathil, C. Pornrungroj, C. D. Sahm and E. Reisner, *Nat. Catal.*, 2022, **5**, 633.
86 N. Wen, Q. Jiang and D. Liu, *Sci. Adv.*, 2024, **10**, eadp8567.
87 S. Günes, H. Neugebauer and N. S. Sariciftci, *Chem. Rev.*, 2007, **107**, 1324.
88 G. Li, V. Shrotriya, J. Huang, Y. Yao, T. Moriarty, K. Emery and Y. Yang, *Nat. Mater.*, 2005, **4**, 864.
89 N. Wen, Q. Jiang, J. Cui, H. Zh, B. Ji and D. Liu, *Nano Today*, 2022, **47**, 101681.
90 S. Tamang, C. Lincheneau, Y. Hermans, S. Jeong and P. Reiss, *Chem. Mater.*, 2016, **28**, 2491.
91 M. Rafipoor, H. Tornatzky, D. Dupont, J. Maultzsch, M. D. Tessier, Z. Hens and H. Lange, *J. Chem. Phys.*, 2019, **151**, 154704.
92 M. D. Tessier, D. Dupont, K. De Nolf, J. De Roo and Z. Hens, *Chem. Mater.*, 2015, **27**, 4893.
93 Y. Ding, J. R. Bertram, C. Eckert, R. R. Bommareddy, R. Patel, A. Conradie, S. Bryan and P. Nagpal, *Energy Environ. Sci.*, 2019, **141**, 10272.
94 C. Liu, J. J. Gallagher, K. K. Sakimoto, E. M. Nichols, C. J. Chang, M. C. Chang and P. Yang, *Nano Lett.*, 2015, **15**, 3634.
95 J. Kim, S. Cestellos-Blanco, Y. X. Shen, R. Cai and P. Yang, *Nano Lett.*, 2022, **22**, 5503.
96 S. Cheemanapalli, R. Mopuri, R. Golla, C. M. Anuradha and S. K. Chitta, *Biomed. Pharmacother.*, 2018, **108**, 547.
97 J. Guo, M. Suástegui, K. K. Sakimoto, V. M. Moody, G. Xiao, D. G. Nocera and N. S. Joshi, *Science*, 2018, **362**, 813.
98 M. Suástegui, C. Yu Ng, A. Chowdhury, W. Sun, M. Cao, E. House, C. D. Maranas and Z. Shao, *Metab. Eng.*, 2017, **42**, 134.
99 R. Hatti-Kaul, U. Törnvall, L. Gustafsson and P. Börjesson, *Trends Biotechnol.*, 2007, **25**, 119.

100 Z. Xiao and J. R. Lu, *Biotechnol. Adv.*, 2014, **32**, 492.
101 S. Maina, A. A. Prabhu, N. Vivek, A. Vlysidis, A. Koutinas and V. Kumar, *Biotechnol. Adv.*, 2022, **54**, 107783.
102 W. Meng, C. Ma, P. Xu and C. Gao, *Trends Biotechnol.*, 2022, **40**, 958.
103 Z. Guo, X. Zhao, Y. He, T. Yang, H. Gao, G. Li, F. Chen, M. Sun, J. K. Lee and L. Zhang, *J. Microbiol. Biotechnol.*, 2016, **27**, 92.
104 M. Otagiri, S. Ui, Y. Takusagawa, T. Ohtsuki, G. Kurisu and M. Kusunoki, *FEBS Lett.*, 2010, **584**, 219.
105 Z. Wang, Q. Song, M. Yu, Y. Wang, B. Xiong, Y. Zhang, J. Zheng and X. Ying, *Appl. Microbiol. Biotechnol.*, 2014, **98**, 641.
106 Y. Tian, Z. Guo, J. He, D. Xu, W. W. Li, S. Cheng and H. Song, *J. CO2 Util.*, 2025, **93**, 103051.
107 B. Fu, X. Mao, Y. Park, Z. Zhao, T. Yan, W. Jung, D. H. Francis, W. Li, B. Pian, F. Salimijazi, M. Suri, T. Hanrath, B. Barstow and P. Chen, *Nat. Chem.*, 2023, **15**, 1400.
108 J. Ackermann, S. Müller, A. Lösche, T. Bley and W. Babel, *J. Biotechnol.*, 1995, **39**, 9.
109 C. R. Hankermeyerand and R. S. Tjeerdema, *Rev. Environ. Contam. Toxicol.*, 1991, **159**, 1.
110 R. T. Chan, R. A. Russell, H. Marçal, T. H. Lee, P. J. Holden and L. J. R. Foster, *Biomacromolecules*, 2013, **15**, 339.
111 E. Markl, H. Grünbichler and M. Lackner, *Novel Tech. Nut. Food Sci.*, 2018, **2**, 1.
112 S. P. Mohandas, L. Balan, N. Lekshmi, S. S. Cubelio, R. Philip and I. S. Bright Singh, *J. Appl. Microbio.*, 2017, **122**, 698.
113 A. A. Alarfaj, M. Arshad, E. N. Sholkamy and M. A. Munusamy, *Braz. Arch. Bio. Tech.*, 2015, **58**, 781.
114 F. A. P. Tassia, L. J. Marcos, D. B. Watanabe, A. Bonomi, L. K. Quines, W. Schmidell and G. M. F. de Aragao, *Bioch. Eng. J.*, 2019, **146**, 97.
115 R. S. Sasidharan, S. G. Bhat and M. Chandrasekaran, *Ann. Microbiol.*, 2015, **65**, 455.
116 A. Pohlmann, W. F. Fricke, F. Reinecke, B. Kusian, H. Liesegang, R. Cramm, T. Eitinger, C. Ewering, M. Pötter, E. Schwartz, A. Strittmatter, I. Voss, G. Gottschalk, A. Steinbüchel, B. Friedrich and B. Bowien, *Nat. Biotechnol.*, 2006, **24**, 1257.
117 C. Liu, B. C. Colón, M. Ziesack, P. A. Silver and D. G. Nocera, *Science*, 2016, **352**, 1210.
118 M. Xu, P. L. Tremblay, L. Jiang and T. Zhang, *Green Chem.*, 2019, **21**, 2392.
119 P. L. Tremblay, M. Xu, Y. Chen and T. Zhang, *iScience*, 2020, **23**, 100784.
120 J. Liu, Y. Zhang, L. Lu, G. Wu and W. Chen, *Chem. Commun.*, 2012, **48**, 8826.
121 J. Liu, Y. Liu, N. Liu, Y. Han, X. Zhang, H. Huang, Y. Lifshitz, S. T. Lee, J. Zhong and Z. Kang, *Science*, 2015, **347**, 970.
122 P. B. Pati, G. Damas, L. Tian, D. L. A. Fernandes, L. Zhang, I. B. Pehlivan, T. Edvinsson, C. M. Araujo and H. Tian, *Energy Environ. Sci.*, 2017, **10**, 1372.
123 W. Yu, M. V. Pavliuk, A. Liu, Y. Zeng, S. Xia, Y. Huang, H. Bai, F. Lv, H. Tian and S. Wang, *ACS Appl. Mater. Interfaces*, 2023, **15**, 2183.
124 Z. Sun, J. A. Ramsay, M. Guay and B. A. Ramsay, *Appl. Microbiol. Biotechnol.*, 2007, **74**, 69.
125 Y. Li, S. Li, K. Qu, J. Yang, S. Wang and Z. Yan, *J. Environ. Sci.*, 2025, 55, DOI: 10.1016/j.jes.2025.07.037.
126 W. Wang, M. Zhang, M. Guo, J. Wang, X. Wang, J. Yin, L. Chen and Y. Li, *Green Chem.*, 2026, **28**, 213.
127 Y. Zheng, L. Lin, B. Wang and X. Wang, *Angew. Chem., Int. Ed.*, 2015, **54**, 12868.
128 W. Wang, H. Zhang, M. Guo, H. Dong, M. Zhang and L. Chen, *ACS Sustainable Chem. Eng.*, 2025, **13**, 7043.
129 Y. Kita, R. Fujii and Y. Amao, *Sustainable Energy Fuels*, 2023, **7**, 360.
130 Y. Kita and Y. Amao, *Catal. Surv. Asia*, 2023, **27**, 67.
131 Y. Kita and Y. Amao, *Chem. Commun.*, 2022, **58**, 11131.
132 Y. Kita and Y. Amao, *Green Chem.*, 2023, **25**, 2699.
133 C. Rosier, N. Leys, C. Henoumont, M. Mergeay and R. Wattiez, *Appl. Microbiol. Biotechnol.*, 2012, **78**, 4516.
134 M. K. Sluis, R. A. Larsen, J. G. Krum, R. Anderson, W. W. Metcalf and S. A. Ensign, *J. Bacteriol.*, 2002, **184**, 2969.
135 T. Katagiri and Y. Amao, *Green Chem.*, 2020, **22**, 6682.
136 Y. Amao, *Sustainable Energy Fuels*, 2018, **2**, 1928.
137 Y. Amao, *Chem. Rev.*, 2026, **126**, 1635.
138 R. Gupta and A. K. Pal, *Sustainable Energy Fuels*, 2024, **8**, 4709.
139 W. Lubitz, H. Ogata, O. Rüdiger and E. Reijerse, *Chem. Rev.*, 2014, **114**, 4081.
140 H. Jia, L. Wanb, Y. Gaoc, P. Duc, W. Lic, H. Luoc, J. Ningc, Y. Zhaoc, H. Wangd, L. Zhangd and L. Zhang, *J. Energy Chem.*, 2023, **85**, 348.
141 S. I. Allakhverdiev, V. D. Kreslavski, V. Thavasi, S. K. Zharmukhamedov, V. V. Klimov, T. Nagata, H. Nishihara and S. Ramakrishna, *Photochem. Photobiol. Sci.*, 2009, **8**, 148.
142 Y. Liu, C. Pulignani, S. Webb, S. J. Cobb, S. Rodríguez-Jiménez, D. Kim, R. D. Milton and E. Reisner, *Chem. Sci.*, 2024, **15**, 6088.
143 K. P. Sokol, W. E. Robinson, J. Warnan, N. Kornienko, M. M. Nowaczyk, A. Ruff, J. Z. Zhang and E. Reisner, *Nat. Energy*, 2018, **3**, 944.
144 C. A. Caputo, L. Wang, R. Beranek and E. Reisner, *Chem. Sci.*, 2015, **6**, 5690.
145 K. A. Brown, S. Dayal, X. Ai, G. Rumbles and P. W. King, *J. Am. Chem. Soc.*, 2010, **13**, 9672.
146 K. W. Brown, M. B. Wilker, M. Boehm, G. Dukovic and P. W. King, *J. Am. Chem. Soc.*, 2012, **134**, 5627.
147 M. B. Wilker, K. E. Shinopoulos, K. A. Brown, D. W. Mulder, P. W. King and G. Dukovic, *J. Am. Chem. Soc.*, 2014, **136**, 4316.
148 Y. Honda, H. Hagiwara, S. Ida and T. Ishihara, *Angew. Chem., Int. Ed.*, 2016, **55**, 8045.
149 Y. Honda, Y. Shinohara and H. Fujii, *Catal. Sci. Technol.*, 2020, **10**, 6006.
150 Y. Honda, M. Yamamoto, Y. Shinohara, Y. Hatanaka, M. Watanabe, T. Ishihara and H. Fujii, *ACS Appl. Nano Mater.*, 2025, **8**, 21294.
151 Y. Amao, *J. CO2 Util.*, 2018, **26**, 623.
152 M. Moon, G. W. Park, J. Lee, J. S. Lee and K. Min, *J. CO2 Util.*, 2020, **42**, 101353.
153 W. Ma, Q. Geng, C. Chen, Y. C. Zheng, H. L. Yu and J. H. Xu, *ChemBioChem*, 2023, **24**, e202300390.
154 A. Maier, L. M. Mguni, A. C. R. Ngo and D. Tischler, *ChemCatChem*, 2024, **16**, e202401021.
155 X. Guo, X. Wang, Y. Liu, Q. Li, J. Wang, W. Liu and Z. K. Zhao, *Chem. – Eur. J.*, 2020, **26**, 16611.
156 D. Mandler and I. Willner, *J. Chem. Soc., Perkin Trans. 2*, 1998, 997.
157 X. Huang, L. Xu, H. Qian, X. Wang and Z. Tao, *J. Nanobiotechnol.*, 2022, **20**, 295.
158 Z. Chi, G. L. Liu, C. G. Liu and Z. M. Chi, *Appl. Microbiol. Biotechnol.*, 2016, **10**, 841.
159 C. M. Krell and D. Seebach, *Eur. J. Org. Chem.*, 2000, 1207.
160 K. Tabata, K. Kasuya, H. Abe, K. Masuda and Y. Doi, *Appl. Environ. Microbiol.*, 1999, **65**, 4268.
161 H. Adelnia, H. D. N. Tran, P. J. Little, I. Blakey and H. T. Ta, *ACS Biomater. Sci. Eng.*, 2021, **7**, 2083.
162 J. J. Pueyo and C. Gömez-Moreno, *Enzyme Microb. Technol.*, 1992, **14**, 8.
163 M. T. Bes, A. L. de Lacey, V. M. Fernandez and C. Gömez-Moreno, *Bioelectrochem. Bioenerg.*, 1995, **38**, 179.
164 Y. Kim, K. Ikebukuro, H. Muguruma and I. Karube, *J. Biotechnol.*, 1998, **59**, 213.
165 H. Inoue, M. Yamachika and H. Yoneyama, *J. Chem. Soc., Faraday Trans.*, 1992, **88**, 2215.
166 K. A. Brown, M. B. Wilker, M. Boehm, H. Hamby, G. Dukovic and P. W. King, *ACS Catal.*, 2016, **6**, 2201.
167 T. Itoh, H. Asada, K. Tobioka, Y. Kodera, A. Matsushima, M. Hiroto, H. Nishimura, T. Kamachi, I. Okura and Y. Inada, *Bioconjugate Chem.*, 2000, **11**, 8.
168 Z. Jiang, C. Lüa and H. Wu, *Ind. Eng. Chem. Res.*, 2005, **44**, 4165.
169 Q. Shi, D. Yang, Z. Jiang and J. Li, *J. Mol. Catal. B*, 2006, **43**, 44.
170 S. H. Lee, D. H. Nam, J. H. Kim, J. O. Baeg and C. B. Park, *ChemBioChem*, 2009, **10**, 1621.
171 J. H. Kim, S. H. Lee, J. S. Lee, M. Lee and C. B. Park, *Chem. Commun.*, 2011, **47**, 10227.
172 Y. Katagiri and Y. Amao, *Sustainable Energy Fuels*, 2022, **6**, 2581.
173 D. H. Nam and C. B. Park, *ChemBioChem*, 2012, **13**, 1278.
174 G. Zhao, C. Yang, W. Meng and X. Huang, *J. Mater. Chem. A*, 2024, **12**, 3209.
175 H. Wu, C. Tian, X. Song, C. Liu, D. Yang and Z. Jiang, *Green Chem.*, 2013, **15**, 1773.
176 Y. Amao and M. Ishikawa, *Catal. Commun.*, 2007, **8**, 523.
177 M. Takeuchi and Y. Amao, *Sustainable Energy Fuels*, 2023, **7**, 355.
178 M. Takeuchi and Y. Amao, *RSC Sustainability*, 2023, **1**, 1874.
179 M. Takeuchi and Y. Amao, *Dalton Trans.*, 2024, **53**, 418.

180 P. H. Wang, K. Correia, H. C. Ho, N. Venayak, K. Nemr, R. Flick, R. Mahadevan and E. A. Edwards, *ISME J.*, 2019, **13**, 1042.
181 M. J. MacDonald, *J. Biol. Chem.*, 1995, **270**, 20051.
182 M. Takeuchi and Y. Amao, *RSC Sustainability*, 2024, **2**, 2491.
183 M. Takeuchi and Y. Amao, *New J. Chem.*, 2024, **48**, 18055.
184 A. Horikawa and Y. Amao, *Energy Fuels*, 2025, **39**, 19537.
185 M. Takeuchi and Y. Amao, *RSC Sustainability*, 2023, **1**, 90.
186 M. Takeuchi and Y. Amao, *New J. Chem.*, 2023, **47**, 17679.
187 I. A. Rose, J. V. B. Warms and D. J. Kuo, *Biochemistry*, 1992, **31**, 9993.
188 I. A. Rose, J. V. B. Warms and R. G. Yuan, *Biochemistry*, 1993, **32**, 8504.
189 S. Beeckmans and E. van Driessche, *J. Biol. Chem.*, 1998, **273**, 31661.
190 M. Takeuchi and Y. Amao, *J. Jpn. Petrol. Inst.*, 2024, **67**, 167.
191 G. Li, Z. Lin, X. Li, Y. Zhang, W. Zhu, Y. Shao, Q. Xue, Q. Fan, T. Tan and H. Cao, *J. Mater. Chem. A*, 2024, **12**, 192.
192 S. K. Guttikunda and P. Jawahar, *Atmos. Environ.*, 2014, **92**, 449.
193 V. B. Y. Oh, S. F. Ng and W. J. Ong, *J. Cleaner Prod.*, 2022, **379**, 134673.
194 S. Das, S. Das, M. M. Ghangrekar and B. Min, *J. Environ. Chem. Eng.*, 2025, **13**, 119221.

